DOI:10.14753/SE.2022.2679

SEMMELWEIS EGYETEM

DOKTORI ISKOLA

Ph.D. értekezések

2679.

PROKOP SUSANNE CLARA

Neuromorfológia és sejtbiológia
című program

Programvezető: Dr. Alpár Alán, egyetemi tanár

Témavezető: Dr. Katona István, tudományos tanácsadó

DOI:10.14753/SE.2022.2679

Advanced fluorescent ligand-based techniques for the pharmacological and anatomical investigation of dopamine receptors

PhD thesis

Susanne Prokop

János Szentágothai Doctoral School of Neurosciences

Semmelweis University

Supervisor: István Katona, DSc

Official reviewers: Katalin Schlett, PhD
Zoltán Varga, PhD

Head of the Complex Examination Committee: Alán Alpár, DSc

Members of the Complex Examination Committee: Miklós Réthelyi, DSc
Ádám Dénes, PhD

Budapest
2022

DOI:10.14753/SE.2022.2679

Table of Contents

DOI:10.14753/SE.2022.2679

DOI:10.14753/SE.2022.2679

List of Abbreviations

3D	three-dimensional
ANOVA	analysis of variance
APD	antipsychotic drug
Axon Term.	axon terminal
BRET	bioluminescence resonance energy transfer
CNS	central nervous system
C	caudal
CAR	cariprazine
CP	caudoputamen
D	dorsal
DAPI	4′,6-diamidino-2-phenylindole
DARPP-32	dopamine- and cAMP-regulated phosphoprotein of molecular weight 32,000
D_1R	D_1 dopamine receptor
D_2R	D_2 dopamine receptor
D_3R	D_3 dopamine receptor
DR	dopamine receptor
DS	dorsal striatum
EC_{50}	half maximal effective concentration
Fig.	Figure
Fluo-CAR	cariprazine labeled fluorescently with Sulfo-Cy5
FRET	fluorescence resonance energy transfer
GLuc-PM	Gaussia-luciferase targeted to the cell surface
GPCR	G protein-coupled receptor
HA	hemagglutinin
IC_{50}	half maximal inhibitory concentration
IoC	Islands of Calleja
K_D	dissociation constant
k_{off}	dissociation rate constant
KO	knockout

DOI:10.14753/SE.2022.2679

k_{on}	association rate constant
LP	localization point
NAc	nucleus accumbens
norm.	normalized
n.s.	not significant
PFC	prefrontal cortex
Preterm. Axon	preterminal axon
R	rostral
rel.	relative
RET	resonance energy transfer
S.E.M.	standard error of the mean
SMLM	single-molecule localization microscopy
STORM	stochastic optical reconstruction microscopy
TH	tyrosine hydroxylase
V	ventral
Veh	vehicle
VS	ventral striatum
WT	wild type

DOI:10.14753/SE.2022.2679

1. Introduction

G protein-coupled receptors (GPCRs) represent the largest and most diverse family of plasma membrane receptors. They serve as the major targets of currently applied clinical drugs and continued efforts are underway to expand the current set of GPCR ligands for therapeutic purposes[1, 2]. Accordingly, an extensive variety of experimental approaches has been developed to study the ligand recognition process and signaling mechanisms of GPCRs.

1.1. Classical radioligand-based assay in GPCR research

Radioligands represent the traditional as well as the most-widely used research tools for ligand binding studies[3, 4]. Conventionally, the key quantitative parameters describing receptor-radioligand interactions are measured in homogenized membrane preparations obtained from cell cultures or tissue samples. These include the dissociation constant (K_D), that is applied to characterize the receptor affinity of a radioligand in equilibrium state, and kinetic binding parameters, such as the association and dissociation rate constants (k_{on} and k_{off}, respectively). In competitive radioligand binding studies, these parameters can be determined for any non-labeled drugs that bind the same receptor as the radioactive compound. Since the maximal amount of bound ligands (B_{max}) is indicative of the number of receptors, saturation binding assays with selective ligands are also suitable for describing the expression level of specific GPCRs in different cell culture- or tissue membrane preparations[4].

In addition to *in vitro* pharmacological measurements, radioligands can be applied as efficient anatomical labeling probes in tissue samples. In these experiments, radioligands bind receptor targets at their native localization sites on anatomical sections and the distribution pattern of radioactive decay can be visualized on autoradiographs[5, 6]. Certainly, radioligand-based localization maps of GPCRs are of outstanding significance, since numerous receptors, including important clinical drug targets, cannot be selectively visualized in tissue preparations by other routinely applied labelling tools due to the lack of selective probes.

Overall, the contribution of radioligands to our current understanding of pharmacological principals can hardly be overemphasized. However, despite of their substantial contribution to the development of research compounds and clinical drugs, radioassays still face major limitations. Here, I highlight the issues that complicate currently applied radioligand-based experiments or leave some of the most emerging questions of modern pharmacological research unanswered.

In classical *in vitro* binding assays, unbound radioligands need to be separated before counting the scintillation of receptor-bound molecules[7–9]. The complications of the separation process, coupled with the relatively low signal-to-noise ratio and high well-to-well variety hinder the adaptation of these assays to high-throughput screening platforms. Another obstacle is that the ratio of ligand-occupied receptors needs to be determined at separate assay points to decipher kinetic binding data and live cell real-time measurements are unobtainable[7, 9]. Scintillation proximity assays do not require the separation of free radioligands, and thus overcome several limitations of traditional binding studies[8]. However, despite of a series of technical improvements, radiometric high-throughput assays and kinetic measurements have remained burdensome for many pharmacologically important GPCRs[8, 9].

Regarding autoradiography, a major constraint is the generally poor spatial resolution of the image that only permits region-specific analysis of drug-target interactions. In contrast, the same receptor-ligand interaction within a specific anatomical area can regulate a wide array of physiological mechanisms, depending on its cell-type specific localization. Moreover, the subcellular localization of a receptor determines the precise composition of the local signaling machinery that can be activated upon ligand binding. Therefore, it remains difficult to draw conclusion about the functional effects of a ligand from its region-wide distribution. Accordingly, the ability of an autoradiograph to directly predict the specific molecular changes that underly the effects of a radiolabeled therapeutic is highly limited.

Another weakness of autoradiography is that autoradiographs are inherently single channel images. Therefore, the lack of additional spatial markers on the sections hinders the analysis of the ligand binding pattern within a well-defined anatomical context. Finally, the general safety concerns regarding radioactivity greatly hinders the wide-

spread application of radioligands and have long encouraged researchers to replace them with more environmentally-friendly tools[10].

1.2. Emerging applications of fluorescent drugs for studying receptor-ligand interactions

Numerous pharmacological studies have successfully performed quantitative measurements with fluorescently labeled drugs as alternatives to radioligand binding assays. Moreover, they highlighted several complementary advantages of fluorescence methods[9–12]. Fluorescence approaches are more convenient for precise kinetic ligand binding measurements than conventional radioassays since the dynamic changes of fluorescence can be readily monitored by fluorimeters, microscopes, or flow cytometers in real-time[9, 11, 12] . Thus, these approaches have the potential to investigate binding events on short timescales. Furthermore, analogously to competitive radioligand binding measurements, the binding parameters of non-labeled compounds can be assessed in displacement assays.

In quantitative fluorescent binding assays, the amount of receptor-bound ligands is usually either determined via the direct measurement of fluorescence intensity or by the detection of resonance energy transfer (RET) between a labeled receptor and its fluorescent ligand[9–12]. A major advantage of the latter approach is that RET-based platforms are “proximity-based”, as energy transfer is highly dependent on the molecular distance between the energy donor and acceptor (<10 nm) [13–15]. The phenomenon of fluorescence RET (FRET) occurs between a pair of fluorophores after the donor is excited with an external light source. All main GPCR ligand binding parameters could be determined by various FRET and time-resolved FRET assay formats that utilized fluorescent pharmacons with excellent signal-to noise ratio[9, 10, 16]. In the case of bioluminescence resonance energy transfer (BRET), energy is produced by an oxidative reaction of a luciferase enzyme that excites a nearby fluorophore with an appropriate fluorescence spectrum[13]. The fact that BRET does not require extrinsic excitation, circumvents many issues caused by the external illumination of the sample, such as autofluorescence, photobleaching or direct cross-excitation of the acceptor. Due to its small molecular weight and exceptional brightness, the deep sea shrimp *Oplophorus*

gracilirostris-derived NanoLuc is the preferentially applied donor enzyme in BRET-based ligand binding assays, and the fluorescently labeled receptor ligand serves as the energy acceptor[9, 14, 17].

A key drawback of most RET-based ligand binding assays is that they require the covalent tagging of receptors, which may result in incorrect receptor folding and decreased cell-surface expression or may directly affect its ligand binding properties[14, 18, 19]. Another important issue that might hinder the broad implementation of RET-based ligand binding measurements is their relatively high cost, which also limits their adaptation to high-throughput platforms.

Fluorescent small molecules have also been applied for the microscopic investigation of GPCRs in cell culture and tissue samples. In general, fluorescence microscopic techniques have higher spatial resolution than autoradiographs, and multi-channel imaging can be easily performed within the same sample. The lateral- and axial resolutions of high-power confocal microscopic images are ~200 nm and ~500 nm respectively. Moreover, the recent advent of fluorescence super-resolution imaging techniques has enabled the localization of fluorescent molecules even with nanometer precision[20, 21]. Numerous different technical innovations have been introduced to overcome the diffraction limit of light and have become broadly adopted in neuroscientific research. Single-molecule-localization microscopy (SMLM) represents a group of methods which provide one of the highest resolution images. During SMLM experiments, only a subset of the fluorohpores in the sample are detected at each camera frame, and the localization of all emitters are finally computationally reconstructed from a sequence of frames. In the case of stochastic optical reconstruction microscopy (STORM), the temporally separate detection of emitters is achieved by special fluorescent dyes, that can transit between on- and off states. This way, STORM has the capacity to visualize single fluorescent molecules at the nanoscale level and has become widely used for the anatomical localization of labeled proteins in cell-cultures and tissue samples a well. STORM experiments have greatly contributed to our general understanding about the molecular organization of synaptic signalosomes in the brain, the nanoscale arrangements of scaffold proteins, and the dynamics of the cytoskeletal network[22–24]. Despite of the intriguing possibility to visualize single fluorescent drug molecules, GPCR

studies do not routinely integrate STORM imaging into the characterization process of pharmacological interactions, yet.

Consequently, the visualization of pharmacological probes by multi-channel high-resolution microscopy would be a promising new strategy for the cell-type specific analysis of drug binding sites within well-defined molecular complexes. On the other hand, despite of the great potential, fluorescent GPCR ligands are not routinely considered for anatomical purposes[25]. Therefore, the capacity of labeled small molecules for the high-resolution analysis of drug binding sites within complex tissue samples has remained unexploited.

1.3. Rising demand for advanced technical approaches for the investigation of dopamine receptors

1.3.1. Dopamine receptors - key neuropharmacological targets

The demand for advanced experimental approaches to understand ligand-binding interactions is exceptionally high in the case of centrally expressing GPCRs. The immense anatomical complexity coupled with the temporal dynamics of physiological processes in the brain poses outstanding technical challenges that cannot be addressed by conventional ensemble methodologies[26, 27]. As a result, the exact pharmacodynamic mechanisms of numerous neuropsychiatric therapeutic agents, including long-standing clinical drugs, have remained elusive.

The increasing pressure to utilize advanced methodologies for the investigation of centrally acting compounds can be well demonstrated by the large number of remaining questions regarding the mechanism of routinely applied dopamine receptor targeting drugs. Dopamine receptors (DRs) are among the most extensively studied GPCRs in the central nervous system, and their dysregulation has been shown to play major roles in the pathophysiology of multiple neuropsychiatric diseases, including addiction, schizophrenia and Parkinson’s disease[28, 29]. Accordingly, DR-targeting drugs represent a mainstay for the treatment of mental illnesses for decades.

In humans, five genes are known to encode dopamine receptors, that can be classified into two groups based on their pharmacological and structural properties[30]. D_1-like receptors (D_1 and D_5 dopamine receptors) elevate intracellular cAMP concentration upon agonist binding via the activation of $G_{\alpha s/olf}$ proteins, and their structural hallmark is a relatively long C-terminus. The subfamily of D_2-like dopamine receptors includes D_2, D_3 and D_4 receptor subtypes, which inhibit cAMP production via coupling to $G_{i/o}$ proteins, and display higher affinity towards their endogenous ligand, dopamine, than D_1-like receptors. In addition to G proteins, dopamine receptors are also known to mediate intracellular signaling effects via other transducers, including β-arrestins[30]. Out of all five dopamine receptors, D_1 dopamine receptor (D_1R) is the most abundant subtype throughout the human brain. The selective modulation of D_1Rs has been shown to be a successful strategy to treat motor symptoms of Parkinson's disease as well as to ameliorate cognitive impairments[31]. Despite of the huge neuropharmacological potential of D_1R agonists, there are currently no drugs in clinical use which target centrally expressing D_1Rs. Several attempts have been made to apply D_1R-selective ligands as neuropsychiatric therapeutics, however, all failed in preclinical or clinical stages due to the disadvantageous pharmacochemical properties of these compounds. To overcome these limitations, numerous new chemical compounds with different scaffolds and functional effects are currently under investigation and offer new opportunities to develop centrally acting D_1R targeting drugs[31]. On the other hand, there is a broad array of medications that preferentially target D_2-like dopamine receptors. Several small molecules, with completely different functional effects, are being used, including full agonists, partial agonists as well as antagonists. Based on their indications, they can be classified as antiparkinsonian agents, prolactin inhibitors, antiemetics and antipsychotic drugs (APDs)[30]. Traditionally, APDs are further divided into typical (also known as first generation) and atypical (also known as second generation) drugs. Typical APDs are efficacious D_2 dopamine receptor (D_2R) antagonists, which have been applied from the 1950s as tranquillizers and antipsychotic agents[32]. They effectively treat psychotic symptoms of schizophrenia, but often fail to manage the negative symptoms of the disease and may exert severe D_2R-mediated side effects, such as extrapyramidal symptoms or hyperprolactinaemia. The term "atypical APDs" cover a huge set of D_2R antagonists and partial agonists with different clinical efficacy and side effect profiles[32,

33]. Generally, they are considered to mitigate negative symptoms more potently than typical APDs and display a lower risk to cause extrapyramidal symptoms. Certainly, all antipsychotic drugs (APDs) are typically “dirty” drugs, meaning that they exert their clinical effects via several different receptor subtypes[32, 34]. However, D_2Rs preserved their leading role, and prominent D_2R affinity has remained a common fundamental feature among typical and atypical APDs.

1.3.2. New aspects of drug-dopamine receptor interactions

Plenty of radioactive and fluorescent small molecules have been previously applied to investigate the ligand binding mechanisms of DRs in cell culture and tissue experiments [35, 36]. Notably, labeled therapeutic drugs have historical importance in dopamine receptor research. The first experimental evidence that D_2 dopamine receptors are the underlying molecular players of antipsychotic action was provided by radioligand binding studies with tritiated haloperidol[37]. This finding solidified the dopaminergic hypothesis of schizophrenia and provided the basis for a great collection of other medications[37].

Although APDs are classically used in the management of schizophrenia or other psychotic disorders, they are also effective in a range of additional illnesses, such as affective disorders[38, 39]. Here, I briefly illustrate the critical importance of accurate *in vitro* ligand-binding assays and the need for novel cell-type-specific approaches by summarizing the findings in two recent studies that analyzed D_2R mediated actions of APDs.

Perhaps the most elegant demonstration of the clinical significance of comprehensive *in vitro* binding studies was shown by correlating the kinetic D_2R binding parameters of APDs with their clinical side-effect profiles[39]. The kinetics of receptor-ligand binding was assessed by a competitive time-resolved FRET assay that applied a fluorescently labeled D_2R agonist as tracer[39, 40]. Thereafter, the time course of receptor-APD interactions were correlated with the classic adverse effects of APD treatment, including hyperprolactinemia and extrapyramidal motor symptoms, both mediated by D_2Rs. It was found that the extent of prolactin elevation negatively correlates

with the k_{off} values of APDs, but the occurrence of extrapyramidal symptoms positively scales with their k_{on} rates[39].

The necessity of region- and cell-type-specific pharmacological measurements was illuminated by the discovery that the recruitment of distinct intracellular signaling machineries can underlie different behavioral effects of D_2R activation in two different brain regions[41]. The effects of a β-arrestin2-biased D_2R partial agonist in the prefrontal cortex (PFC) and the striatum were compared in a series of behavioral and electrophysiological assays. Due to the higher G protein-coupled receptor kinase 2 and β-arrestin2 expression in the PFC, agonist-like effects of the drug dominated in PFC fast-spiking interneurons but not in striatal medium spiny neurons[41].

As these two studies above highlighted, the precise spatiotemporal aspects of APD-D_2R binding have critical importance in the clinical effects of these therapeutics. An additional factor which contributes to the complexity of APDs' mechanism of action is that many APDs modulate the dopaminergic system via D_2 and D_3 dopamine receptors (D_3Rs) as well, due to the remarkable structural homology between the two receptor subtypes. Moreover, the expression pattern of the receptor proteins is overlapping in many brain areas, although D_2Rs are substantially more abundant. The similarity of their ligand binding pockets often results in similar affinities of drugs to both subtypes and suggests that the role of D_3Rs in the action of APDs cannot be ignored. Importantly, a rapidly emerging APD, cariprazine, displays strong preference towards the D_3 receptor subtype over the classical antipsychotic target, D_2R[42, 43]. The drug's special pharmacological profile is accompanied by unique clinical effects: cariprazine displays exceptional efficacy in the management of negative symptoms and its long-term use capably prevents relapse in patients with schizophrenia[44–46]. Furthermore, cariprazine has been recently approved for the treatment of bipolar I disorder as well. Rodent behavioral models have suggested that several effects of the drug are mediated by D_3 receptors[47, 48]. However, the precise neuroanatomical localization of cariprazine binding sites in the brain has not been investigated before, and its exact mechanism of action remained elusive.

Taken together, the expanding set of APDs, together with the temporal dynamics of the dopaminergic system and the brain-wide expression of DRs in various cell-types warrant advanced methodologies to investigate the mechanisms of DR-targeting drugs.

DOI:10.14753/SE.2022.2679

Presumably, the large number of well-characterized dopamine receptor targeting radioligands will continuously provide support. Meanwhile, the expanding set of fluorescent DR ligands can further help to shed light on the puzzling questions about the pharmacology of DRs[15, 49–52].

DOI:10.14753/SE.2022.2679

2. Objectives

In light of the rising demand for improved experimental approaches to investigate emerging aspects of receptor-ligand interactions, we aimed to broaden the applicability of fluorescent pharmacoprobes and develop refined fluorescent small molecule-based assays.

Considering the leading role of DRs in the pharmacological management of psychiatric diseases, we decided to apply fluorescently labeled DR ligands to introduce our novel technical approaches and make an assessment about our advancements by the investigation of prototypical D_1- and D_2-like dopamine receptors. We set two specific aims that cover the development of two novel methodologies, which can address major constraints of previous technical approaches and may open up new possibilities for the investigation of pharmacological interactions.

First, our aim was to develop a cost-effective ligand binding assay that facilitates the feasibility of equilibrium and kinetic ligand binding measurements. Within the confines of this objective, we aimed to investigate the prototype of the D_1-like dopamine receptor subfamily, D_1R. We selected a commercially available fluorescent D_1R ligand that possess optimal photochemical properties for bioluminescence resonance energy transfer (BRET) assays. We hypothesized that ligand-D_1R binding could be measured by detecting bystander BRET between the labeled ligand (acceptor) and a plasma membrane-anchored BRET donor. This way, our platform could offer the intriguing possibility to obtain precise binding parameters of D_1R without its genetic modification Moreover, if our assay is suitable for competitive ligand binding measurements, it could be applied for ligand screening with unmodified dopamine receptors in the future.

Since nanoscale biochemical processes can determine the physiological or pathophysiological effects of receptor-ligands interactions in a cell-type specific manner, our second objective was to develop a novel methodology that enables the analysis of receptor binding in a precise anatomical context, on identified cell types. More specifically, our intention was to design a framework in which we can visualize the receptor engagement of an APD even at the nanoscale level by its fluorescently labeled analogue. We chose a novel, D_3R-preferring third generation APD, cariprazine, as the basis of a novel microscopic pharmacoprobe. We hypothesized that a fluorescently

labeled analogue of cariprazine would be an advantageous research tool for multiple purposes. First, due to its high D_3R affinity, it would represent an exceptionally useful labeling tool, since the D_3R subtype is hard to selectively visualize by other affinity probes. Second, the identification of nanoscale cariprazine binding sites in brain tissue could reveal important details about its hitherto enigmatic mechanism of action. To achieve these results, we decided to optimize a procedure for the multi-channel imaging of fluorescent cariprazine together with functionally related proteins in the same tissue samples and carry out simultaneous multi-target analysis with combined pharmaco- and immunolabeling techniques. Additionally, we aimed to test the feasibility of cell-type specific super-resolution imaging of drug binding sites.

DOI:10.14753/SE.2022.2679

3. Results

3.1. Quantitative ligand binding measurement of D_1 dopamine receptor using Gaussia-BRET

Our first set of experiments aimed to test the utility of a novel BRET-based assay for the quantitative characterization of D_1R ligand binding[53]. In contrast to previous BRET-based approaches, which directly measure RET between donor-tagged receptors and their fluorescent ligands, our methodology is based on the detection of bystander BRET[14, 17], which occurs between the receptor-bound fluorescent probes and a novel plasma membrane anchored biosensor (GLuc-PM). The biosensor consists of a mutant form of the small molecular weight luciferase enzyme from marine copepod *Gaussia princeps* that is fused to the transmembrane domain of the platelet-derived growth factor receptor, assuring the extracellular surface localization of the enzyme. In this assay, the binding of the fluorescently labeled ligand to its receptor leads to the elevation of the bystander BRET signal (Figure (Fig.) 1a). On the other hand, co-treatment with a non-labeled receptor ligand displaces the fluorescent ligands from the receptor, thereby prevents the increase of the bystander BRET. Since the extent of bystander BRET is linearly proportional to the amount of receptor-bound acceptors, the ligand binding parameters of the receptor can be readily quantified. Since no receptor modification is needed in our assay, ligand binding of native receptors can be monitored. The execution of the assay is convenient as the BRET signal can be measured in a "mix and measure" fashion, and unbound fluorescent ligands do not need to be separated. Moreover, the Gaussia-luciferase-based biosensor uses coelenterazine as a substrate for the luciferase reaction, making our measurements exceptionally cost-effective compared to previous BRET assays, which usually apply NanoLuc enzyme with a more expensive substrate (furimazine)[9, 14, 17]. To illustrate the potential of the novel approach for dopamine receptor research, we performed ligand-binding measurements to detect ligand binding of untagged D_1R. Treatment with BODIPY-FL-SKF-83566, a commercially available fluorescent D_1R drug, led to an increase of the BRET ratio in cells co-expressing D_1R and the GLuc-PM, reflecting the binding of the fluorescent ligand to its receptor (Fig. 1b). The specificity of the interaction was proven by a competition binding experiment. Co-treatment with a non-labeled D_1R antagonist (SCH-23390) decreased the BRET signal in

DOI:10.14753/SE.2022.2679

a concentration-dependent manner, and the half maximal inhibitory concentration (IC_{50}) value of SCH-23390 was successfully assessed from the displacement assay (1.07 nM). Since the Gaussia-BRET approach has been shown to be exceptionally advantageous for real-time ligand binding measurements and can be readily adapted to a high-throughput format, our results open up new opportunities for the comprehensive characterization and screening of dopamine receptor targeting drugs[53].

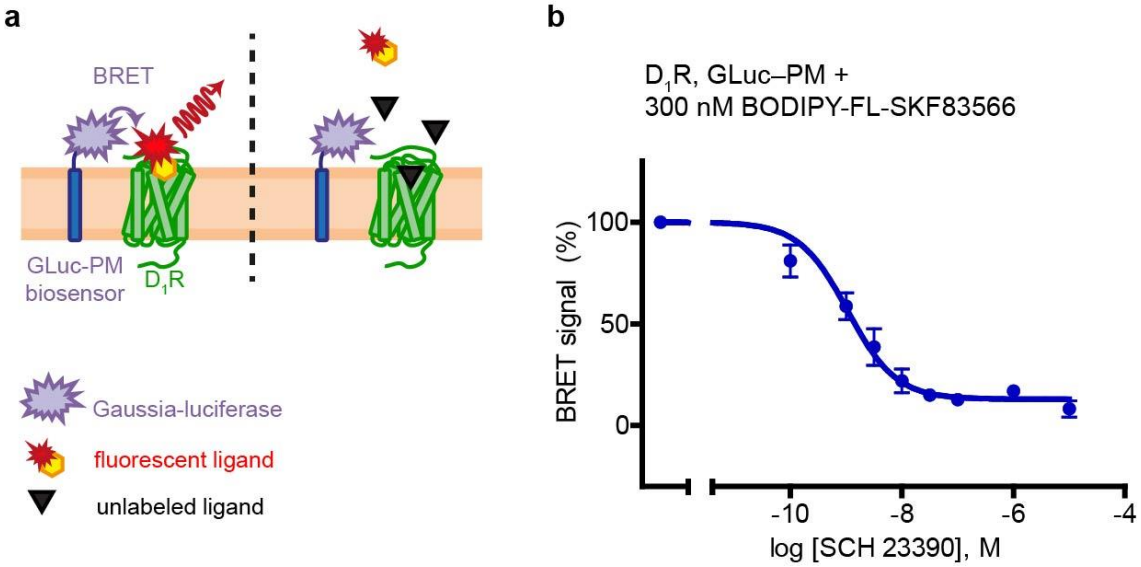

Figure 1. Quantifying D_1R ligand binding with a fluorescent ligand in a novel BRET-based assay. (a) *Schematic illustration of the experimental approach*[53]*. Bystander BRET is measured between receptor-bound fluorescent ligands and a Gaussia-luciferase-based biosensor (GLuc-PM) at the extracellular surface of the plasma membrane. Binding of the fluorescent ligand to its receptor increases the BRET ratio, whereas the displacement of the fluorescent tracer by an unlabeled drug prevents the BRET signal.* ***(b)*** *Demonstration of the feasibility of ligand binding measurement with unmodified D_1Rs in the assay format from (a). HEK 293 cells expressing the GLuc-PM biosensor and human D_1R were incubated with 300 nM BODIPY-FL-SKF83566 and different concentrations of a potent D_1R ligand, SCH 23390. The unlabeled drug decreased the BRET signal in a concentration-dependent manner. IC_{50} value of SCH 23390 was assessed from a one-site competitive binding curve (n = 3), data are mean ± standard deviation.*

3.2. Visualization of receptor binding of an antipsychotic medication by PharmacoSTORM

3.2.1. Rational design and *in vitro* microscopic applications of a fluorescent cariprazine analogue

Radioactive analogues of clinically used drugs have long been applied to investigate their mechanism of actions. On the other hand, the production of fluorescently labeled drugs with pharmacological characteristics that closely resemble the properties of the original compound represents a considerable pharmacochemical challenge. However, recent breakthrough results of the field of GPCR structural biology together with robust computational approaches can provide substantial support for the rational design of novel fluorescently labeled drugs[54–57]. To fulfil our second objective and exemplify the diverse applicability of fluorescent GPCR ligands for microscopic studies, we first aimed to develop a novel pharmacological probe based on an antipsychotic drug, cariprazine. We hypothesized that a fluorescent cariprazine derivative could elucidate the molecular pharmacodynamic actions that underly its remarkable clinical success. Furthermore, it could be an advantageous anatomical research tool for its highest affinity target, the D_3 dopamine receptor subtype[42], which is hard to selectively visualize by other affinity probes. The primary objective during the rational design of the labeled cariprazine was to preserve the main pharmacological properties of the original drug and to keep its strong preference towards D_3R. Shortly, we built a D_3R homology model based on a serotonin 1B receptor structure[58, 59], performed molecular docking simulations to optimize the site of chemical modifications and synthesized the rationally designed compound (Fig. 2a). Cariprazine was equipped with a short molecular linker and with a highly hydrophilic analogue of the most popular cyanine dye for single molecule localization microscopy (SMLM) experiments (Sulfo-Cy5). Firstly, we tested the pharmacological properties of the novel probe (Fluo-CAR) by *in vitro* radioligand binding and BRET-based functional assays. These validated the remarkable pharmacological similarity between Fluo-CAR and the original antipsychotic drug, as it preserved its outstandingly high affinity towards D_3R (K_D =1.31 nM)[59] and acted as a weak D_3R partial agonist in a BRET assay for G_{i1} protein activation, a known signaling effector of D_3R (Fig. 2b,c). After the

DOI:10.14753/SE.2022.2679

pharmacological verification, Fluo-CAR was evaluated as a microscopic labeling tool. Firstly, we expressed hemagglutinin (HA)-tagged D_3Rs in HEK 293 cells and simultaneously visualized the Fluo-CAR binding with anti-HA immunolabeling (Fig. 2d). Fluo-CAR displayed remarkable selectivity to HA-D_3R expressing cells, whereas the plasma membrane of untransfected cells were devoid of Fluo-CAR signal. In accordance with the excellent physicochemical properties of Sulfo-Cy5 dye for SMLM, we were able to detect receptor-bound Fluo-CAR molecules with nanoscale precision by STORM super-resolution microscopy (Fig. 2e-i). Moreover, dual-channel STORM imaging of ligand- and antibody-based labeling (Pharmaco- and ImmunoSTORM) could be performed within the same sample. To verify the specificity of the Fluo-CAR-based PharmacoSTORM signal, we conducted a competitive ligand binding experiment with an unlabeled, selective D_3R antagonist (SB277011-A) (Fig. 2e,f). Pretreatment with SB277011-A significantly reduced the number of PharmacoSTORM localization points (LPs) in the plasma membrane of HA-D_3R expressing cells but did not alter the ImmunoSTORM signal.

DOI:10.14753/SE.2022.2679

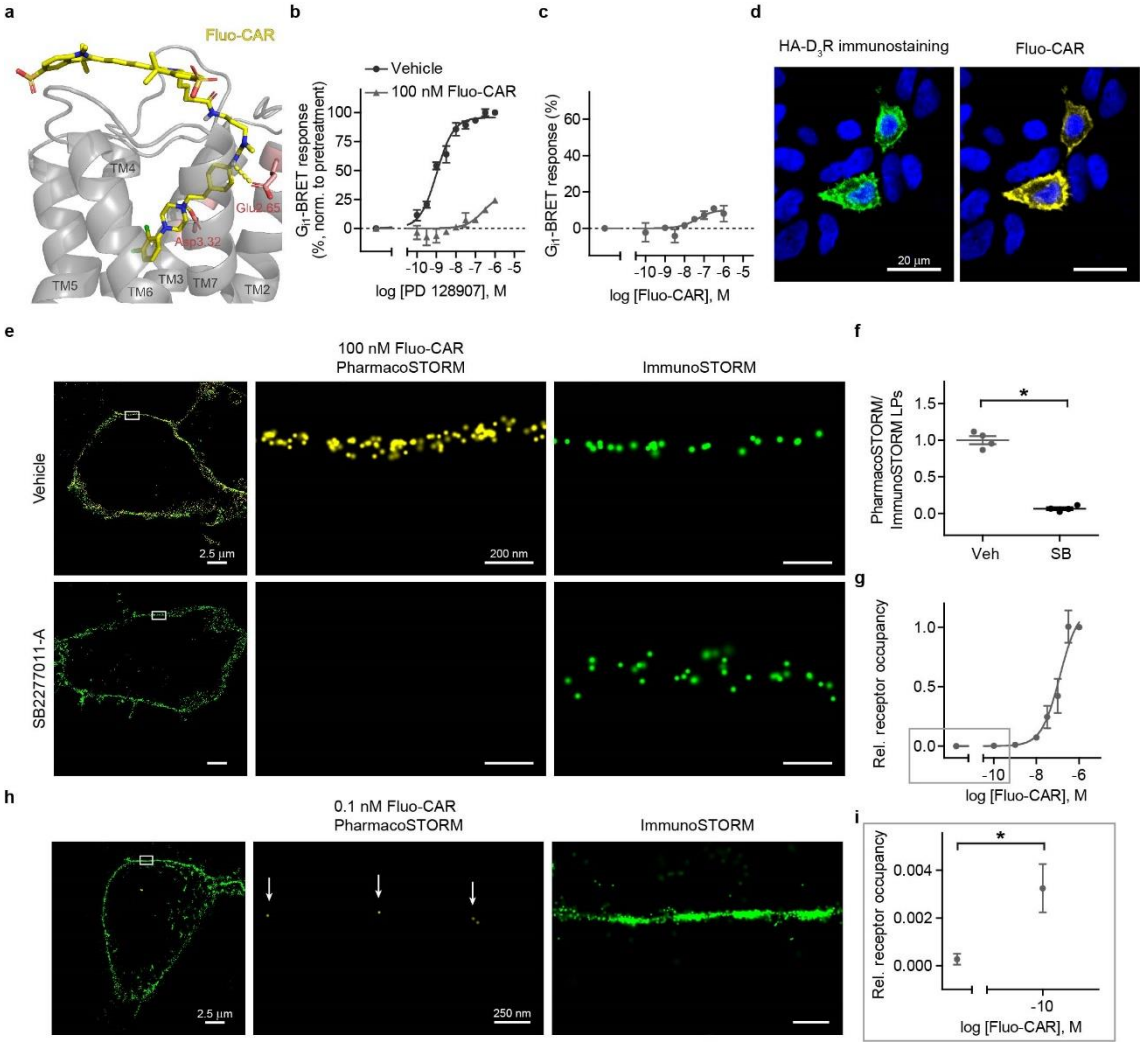

Figure 2. Characterization of fluorescently tagged cariprazine. (a) *The binding pose of cariprazine equipped with a linker and a Sulfo-Cy5 dye (Fluo-CAR, yellow) in a human D_3R (grey) homology model (based on PDB:6G79)*[58]*, obtained by molecular docking simulations. Yellow dashed lines represent the hydrogen bonds between the protein residues (red) and the fluorescent APD analog.* ***(b,c)*** *Functional characterization of Fluo-CAR by a BRET-based in vitro D_3R signaling assay. Receptor activation state was assessed by the extent of RET between donor-tagged $G\alpha_{i1}$ and acceptor-tagged β_1 subunits of G_{i1} heterotrimeric G proteins. Since cariprazine is a partial agonist, the effects of Fluo-CAR were evaluated in both antagonist (b) and agonist (c) assay formats.* ***(b)*** *HEK 293 cells were treated with Fluo-CAR or vehicle before stimulation with D_3R selective agonist PD128907. The concentration-response curve of PD128907 was right-shifted (half maximal effective concentration (EC_{50}) value was increased from 1.047 nM to 256.1 nM (n = 3)) by Fluo-CAR pretreatment.* ***(c)*** *Concentration-response curve of*

Fluo-CAR shows the weak agonistic effects of the novel pharmacoprobe (EC_{50} = 44.1 nm). BRET ratios are normalized (norm.) to the baseline ratios and expressed as the percentage of the signal after 1 μM PD128907 treatment (n = 3). Data are presented as mean ± standard error of the mean (S.E.M.) ***(d)*** *Representative confocal images of combined 22mmune- and pharmacolabeling of N-terminally HA-tagged D_3Rs, expressed in HEK 293 cell culture. Receptors were simultaneously visualized by immunostaining against HA-fusion tag and 100 nM Fluo-CAR treatment, and nuclear staining was performed with 4',6-diamidino-2-phenylindole (DAPI). Fluo-CAR selectively bound cells that expressed the receptor target.* ***(e)*** *Representative dual Pharmaco- and ImmunoSTORM images of HA-tagged D_3Rs in the plasma membrane of HEK 293 cells after 100 nM Fluo-CAR treatment and anti-HA immunolabeling. Pretreatment with a selective D_3R antagonist (10 μM SB277011-A) markedly reduced the density of Fluo-CAR STORM LPs, indicating the specificity of the PharmacoSTORM signal.* ***(f)*** *Quantitative evaluation of the STORM-based competitive ligand binding experiment frI(e). The relative (rel.) receptor occupancy by Fluo-CAR was defined as the ratio of the number of Fluo-CAR STORM LPs and ImmunoSTORM LPs detected in the same membrane segment. To statistically evaluate the reduction of receptor occupancy and thus confirm the selectivity of Fluo-CAR PharmacoSTORM, two-tailed Mann-Whitney test was performed (P = 0.0286, n = 4). Data are presented as mean ± S.E.M, normalized to vehicle pretreatment.* ***(g)*** *Saturation binding curve of Fluo-CAR, assessed by quantitative Pharmaco- and ImmunoSTORM imaging. Receptor occupancy was determined as in (f) and expressed in percentage of the signal after 1 μM Fluo-CAR treatment (n = 3-5). Data were fitted with a one-site sigmoidal binding curve. Half-maximal receptor occupancy was achieved at 124 nM.* ***(h,i)*** *Visualization of low-concentration fluorescent ligand binding. (h). After 0.1 nM Fluo-CAR treatment, individual, sparsely bound Fluo-CAR molecules (white arrows) are detected in the plasma-membrane. (i) Higher magnification of the binding curve from (g) demonstrates the specific detection of receptor-bound Fluo-CAR after 0.1 nM pharmacoprobe treatment. Two-tailed Mann-Whitney U test was performed (P = 0.0294) to confirm significance (n = 3-4). All data are presented as mean ± S.E.M.*

To further challenge the quantitative power of our approach, we performed a conceptually similar experiment as radioligand-based saturation binding assays, but instead of scintillation counting of membrane homogenates, the level of receptor occupancy was evaluated by quantitative dual channel Pharmaco- and ImmunoSTORM imaging of the plasma membrane segments (Fig. 2g-i). Notably, in our high-resolution plasma membrane-delimited saturation binding assay, Fluo-CAR binding to HA-D_3Rs exhibited a classical sigmoidal response function (Fig. 2g). Moreover, in line with the generally high detection sensitivity of SMLM techniques, PharmacoSTORM had the capacity to visualize drug-target interactions at low ligand concentration, and the D_3R binding of separate Fluo-CAR molecules could be specifically detected even at sub-nanomolar concentration (Fig. 2h,i). Altogether, our imaging data obtained from *in vitro* cell cultures provide compelling evidence about the efficiency of quantitative PharmacoSTORM microscopy of rationally designed fluorescent drugs.

3.2.2. Multi-scale imaging of fluorescent cariprazine distribution in the mouse brain

The wide array of fluorescence microscopic techniques offers the possibility to readily visualize the localization of fluorescent molecules at multiple scales. The broad topological distribution of fluorescent drugs can be rapidly analyzed in large sets of tissue samples, whereas super-resolution techniques allow to detect molecules with nanoscale precision. Here, we apply Fluo-CAR to demonstrate that fluorescent-ligand based microscopy can be as useful as autoradiography for the visualization of drug-target interactions at the regional level but brings the additional benefits of high-resolution anatomical measurements. We illustrate these advantages by combining epifluorescence, confocal and STORM microscopy for the multi-scale mapping of Fluo-CAR binding in the mouse brain.

We designed a framework, in which living acute brain slices are treated with a fluorescent pharmacoprobe before chemical fixation and further processed to conform various microscopic settings. Low-magnification epifluorescence images showed highest intensity Fluo-CAR labeling in the ventral part of the basal forebrain (Fig. 3a,b). Closer examination revealed that the fluorescent drug binding sites in this region are mostly

concentrated in the vicinity of dense cell masses, which could be observed throughout all layers of the olfactory tubercle and the ventromedial part of the nucleus accumbens. These cell densities represent the so-called Islands of Calleja (IoC)[60–62]. The islands are formed by the aggregations of small granule cells, and the nearby Fluo-CAR rich areas were identified as “hilar” subregions of the IoC. Despite of the close localization of the islands to the attentively studied ventral striatum, our knowledge about their exact physiological or pathophysiological role is highly limited. Furthermore, open questions remained about their precise anatomical distribution as well. Previous descriptions are highly controversial about the fact, whether these cell masses embody separate independent islands or constitute a single structure presumably due to their complex morphology and lack of reliable selective markers[62–64]. On Fluo-CAR treated coronal brain sections, the prominent pharmacoprobe labeling of the “hilus” often connected separate cell masses (Fig. 3b). This observation encouraged us to perform a precise three-dimensional reconstruction of the Fluo-CAR rich areas from consecutive coronal brain samples (Fig. 3c-e). Indeed, our results corroborated that the IoC represent a continuous structure throughout a surprisingly large portion of the ventral striatum.

DOI:10.14753/SE.2022.2679

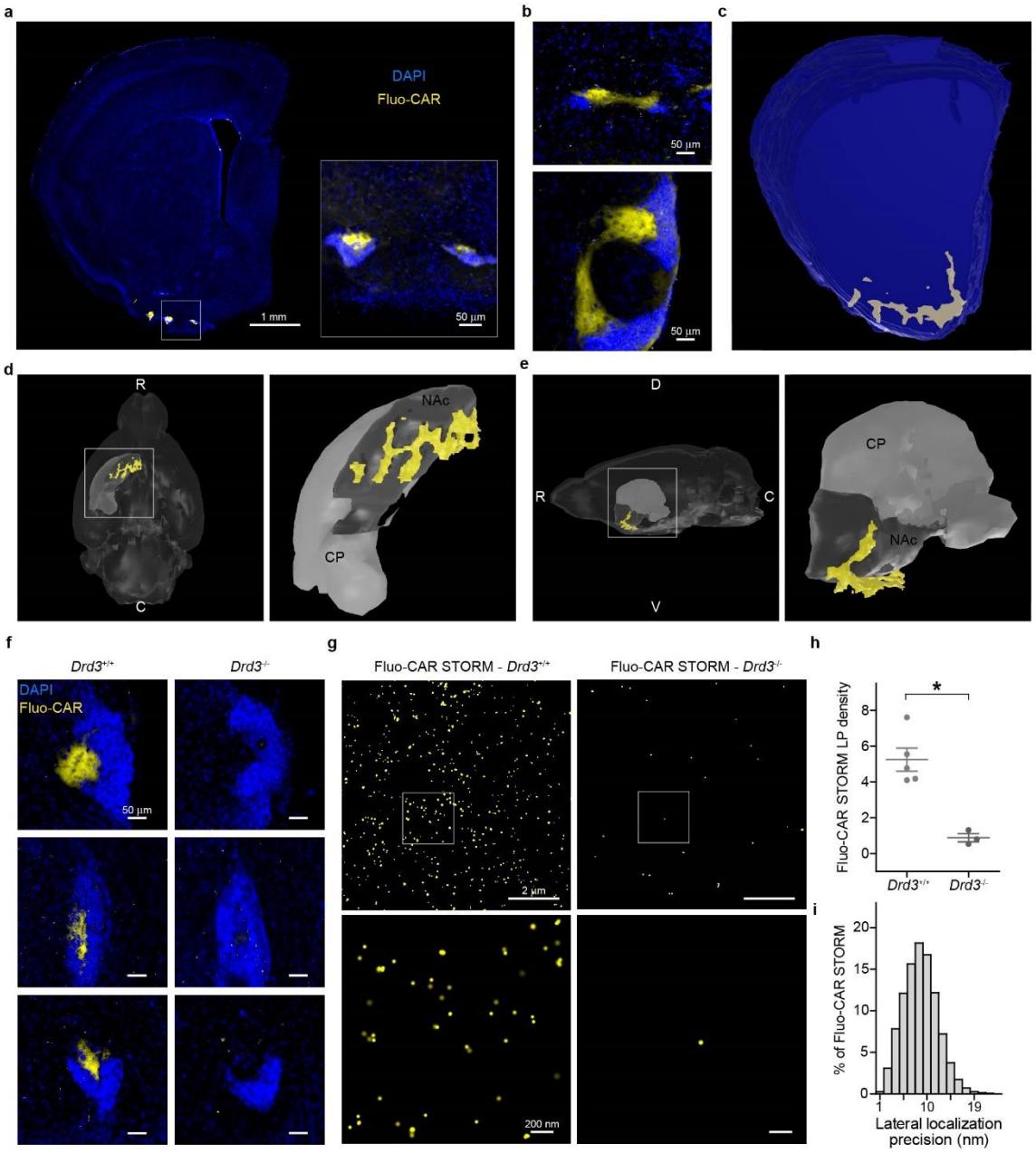

Figure 3. Multi-scale mapping of Fluo-CAR binding in the brain. (a) *Representative epifluorescent image of a coronal mouse forebrain slice, including the ventral and dorsal parts of the striatum as well as the olfactory tubercle, which was recently termed tubular striatum*[65]. *Sections were incubated with 300 nM Fluo-CAR and additional nuclear staining was performed with DAPI. The inset highlights the brain region with the most intense Fluo-CAR labeling. Highest pharmacoprobe density is detected in the so-called hilar subregion of the Islands of Calleja, located in the ventral part of the forebrain.* ***(b)*** *Islands of Calleja are formed by the accumulation of granule cells and appear as distinct cell masses on coronal sections. However, the adjacent Fluo-CAR-rich hilar subregions*

regularly interconnect these structures. ***(c,d,e)*** *Three-dimensional reconstruction of the Islands of Calleja with the help of Fluo-CAR labeling. Precise tracking of areas with dense Fluo-CAR binding sites along consecutive coronal sections reveal that the hilus of the Islands of Calleja represent an unexpectedly large and continuous area. (**d,e**) Ventral (d) and sagittal (e) views of the Fluo-CAR-based anatomical model of the Islands of Calleja (yellow), integrated into a mouse brain atlas. The striatum is displayed alongside in light gray to emphasize the considerable size of this brain region (NAc: nucleus accumbens, CP: caudoputamen). Anatomical directions are indicated by white capital letters. R: rostral, C: caudal, V: ventral, D: dorsal.* ***(f)*** *Representative images of the Islands of Calleja from wild type or D_3R knockout animals ($Drd3^{+/+}$ and $Drd3^{-/-}$, respectively). Acute slices from $Drd3^{+/+}$ and $Drd3^{-/-}$ mice were labeled with Fluo-CAR and processed for microscopy in parallel. Fluo-CAR labelling markedly decreased in the hilus of the entire IoC of $Drd3^{-/-}$ animals. Left images show the rostral extension of the IoC complex, middle images display the so-called major islands, and right pictures exemplify a typical appearance of the caudal part of the IoC in the polymorph layer of the olfactory tubercle.* ***(g)*** *Fluorescent pharmacoprobe-based super-resolution imaging in brain tissue. PharmacoSTORM experiments were performed to visualize Fluo-CAR molecules in the hilus of the IoC of $Drd3^{+/+}$ and $Drd3^{-/-}$ animals after 300 nM Fluo-CAR treatment. In the absence of D_3Rs, the density of Fluo-CAR STORM LPs is dramatically decreased.* ***(h)*** *Statistical comparison of Fluo-CAR binding site density (number of LPs/μm^2) measured in $Drd3^{+/+}$ (n = 5) and $Drd3^{-/-}$ (n = 3) mice by PharmacoSTORM. Two-tailed Mann-Whitney test was performed (P = 0.0357).* ***(i)*** *Lateral localization precision of Fluo-CAR PharmacoSTORM in the Island of Calleja was evaluated by the analysis of the distribution of STORM LPs. The median lateral localization precision was 9.42 nm (n = 98260 LPs).*

In light of the strong *in vitro* preference of Fluo-CAR towards D_3Rs, we tested whether this receptor subtype is the main molecular binding partner of the drug in the IoC. To this end, brain sections from D_3R knockout (KO) animals were labeled and processed in the same manner as the wild type (WT) samples (Fig. 3f-h). In accordance with its receptor affinity profile, Fluo-CAR labeling was fully eliminated from the IoC of D_3R KO animals. These results confirm that the distribution of specific ligand-receptor

interactions can be readily analyzed by fluorescence microscopy. Next, we demonstrated the feasibility of fluorescent ligand-based super-resolution imaging of pharmacological interactions in tissue. We performed STORM experiments with Fluo-CAR in the IoC of D_3R WT and KO mice (Fig. 3g,h). The number of Fluo-CAR LPs was significantly reduced in the absence of D_3Rs, which demonstrated the high specificity of the PharmacoSTORM signal in tissue samples. As opposed to diffraction limited techniques, PharmacoSTORM had the capacity to discern individual fluorescent drug molecules from background and to localize the sites of drug-target interactions with nanoscale precision (median of 9.4 nm at 5 μm tissue depth) (Fig. 3i).

We further challenged the efficiency of our approach and performed PharmacoSTORM nanoscale imaging in striatal regions where Fluo-CAR labeling was substantially weaker than in the IoC based on our diffraction limited microscopic images. Indeed, the number of PharmacoSTORM LP density was significantly lower in the adjacent ventral and dorsal striatum (VS and DS), however, the PharmacoSTORM signal was above the average background level of tissue STORM experiments (Fig. 4a,b). To validate the specificity of the low-density Fluo-CAR signal, we performed a competitive binding experiment, in which unlabeled cariprazine pretreatment of acute slices caused a robust decrease in the number of Fluo-CAR LPs in all areas. In contrast to the IoC, specific Fluo-CAR binding was detected even in the dorsal and ventral striatum even in the absence of D_3Rs (Fig. 4c-f). These results are in agreement with the high expression level of the other lower affinity target of cariprazine, the D_2Rs. These results implicate the feasibility of PharmacoSTORM super-resolution imaging of drug binding sites in tissue areas with substantially different number of receptor targets.

DOI:10.14753/SE.2022.2679

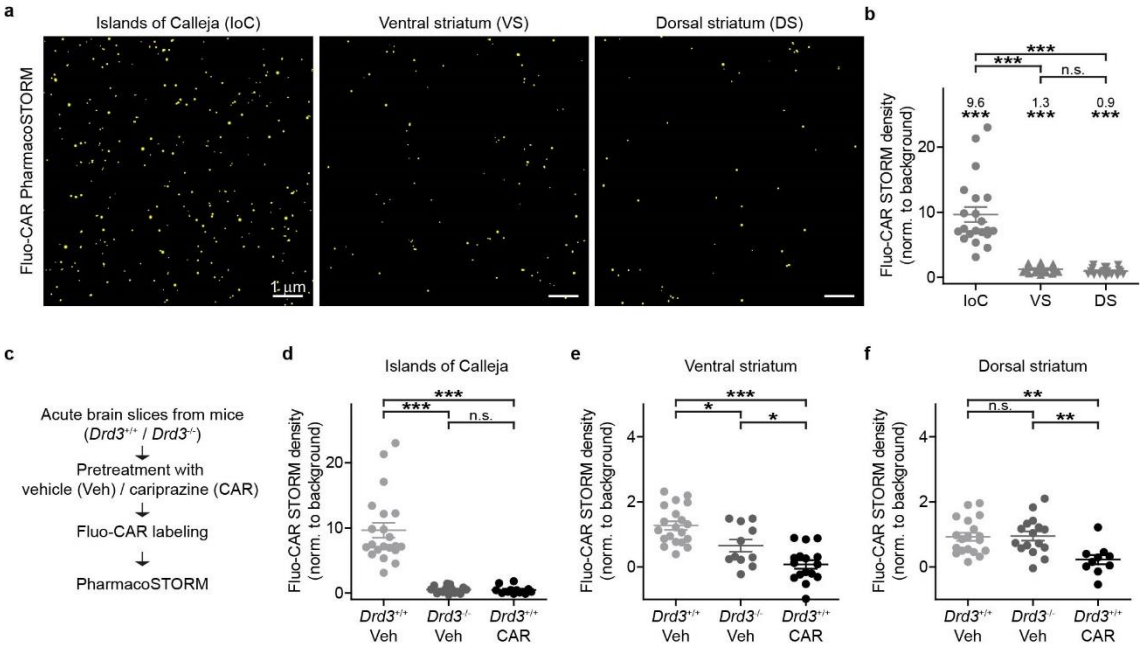

Figure 4. The origin and specificity of Fluo-CAR-based PharmacoSTORM signal in anatomical areas with markedly different drug binding site densities. (a) *Representative PharmacoSTORM images taken in the Islands of Calleja, ventral striatum and dorsal striatum after Fluo-CAR (300 nM)-treatment of mouse coronal brain slices.* ***(b)*** *Verification of the specificity of PharmacoSTORM signal in the selected anatomical areas. The density of Fluo-CAR LPs was normalized to the average STORM background signal (assessed in brain slices without fluorescent drug treatment), then the background was subtracted. Kruskal–Wallis test with Dunn's post-hoc test was performed to statistically confirm the difference between drug binding site densities (IoC vs. VS, ***, $P = 3.34 \times 10^{-6}$; IoC vs. DS, ***, $P = 3.66 \times 10^{-9}$; VS vs. DS, P = 0.6267, not significant (n.s.)). Wilcoxon signed rank test reveals that PharmacoSTORM LP densities were significantly different from 0 even in brain regions with lower density of fluorescent drug binding sites (IoC, n = 21 (from 9 animals), ***, $P = 9.54 \times 10^{-7}$; VS, n = 20 (from 4 animals), ***, $P = 1.91 \times 10^{-6}$; DS, n = 19 (from 4 animals), ***, $P = 3.81 \times 10^{-6}$). Mean values of each group are indicated on the chart.* ***(c)*** *To pharmacologically validate the Fluo-CAR signal based on ligand binding competition, acute slices were pretreated with cariprazine (CAR, 30 µM) or vehicle (Veh). Genetic control experiments were performed to determine the fraction of D_3Rs among the molecular targets of Fluo-CAR in the different brain regions.* ***(d-f)*** *Fluo-CAR signal was markedly reduced by cariprazine pretreatment in all areas, suggesting the specificity of the labeling method.* ***(d)*** *Fluo-CAR*

*binding was abolished in the IoC after cariprazine pretreatment as well as in the absence of D_3Rs. Kruskal–Wallis test with Dunn's post-hoc test was applied ($Drd3^{+/+}$ Veh, n = 21 (from 9 animals); $Drd3^{-/-}$ Veh, n = 13 (from 7 animals); $Drd3^{+/+}$ CAR, n = 12 (from 4 animals); $Drd3^{+/+}$ Veh vs. $Drd3^{-/-}$ Veh, ***, P = 7.72 × 10-6; $Drd3^{+/+}$ Veh vs. $Drd3^{+/+}$ CAR, ***, P = 2.89 × 10-6; $Drd3^{-/-}$ Veh vs. $Drd3^{+/+}$ CAR, P > 0.9999).* ***(e)*** *Fluo-CAR specifically labeled both D_3 and non-D_3 receptor targets in the VS. One-way analysis of variance (ANOVA) with Bonferroni post-hoc tests were performed ($Drd3^{+/+}$ Veh, n = 20 (from 4 animals); $Drd3^{-/-}$ Veh, n = 11 (from 4 animals); $Drd3^{+/+}$ CAR, n = 16 (from 4 animals); $Drd3^{+/+}$ Veh vs. $Drd3^{-/-}$ Veh, *, P = 0.0178; $Drd3^{+/+}$ Veh vs. $Drd3^{+/+}$ CAR, ***, $P = 4.71 \times 10^{-7}$; $Drd3^{-/-}$ Veh vs. $Drd3^{+/+}$ Car, *, P = 0.042).* ***(f)*** *PharmacoSTORM signal was cariprazine-sensitive but was not D_3R-dependent in the dorsal striatum. One-way ANOVA with Bonferroni post-hoc tests were performed ($Drd3^{+/+}$ Veh, n = 19 (from 4 animals); $Drd3^{-/-}$ Veh, n = 16 (from 4 animals); $Drd3^{+/+}$ CAR, n = 10 (from 4 animals); $Drd3^{+/+}$ Veh vs. $Drd3^{-/-}$ Veh, P > 0.9999; $Drd3^{+/+}$ Veh vs. $Drd3^{+/+}$ CAR, **, P = 0.0048; $Drd3^{-/-}$ Veh vs. $Drd3^{+/+}$ CAR, **, P = 0.0047). Data are presented as mean ± S.E.M, dots represent the data of individual images in all panels.*

3.2.3. Combined imaging of pharmacological and anatomical markers

As opposed to autoradiography, fluorescence imaging enables the simultaneous visualization of various proteins of interest, including specific regional and cellular fluorescent anatomical markers. The prevailing technique to delineate distinct brain regions or to differentiate neuronal cell types is immunostaining. Therefore, we hypothesized that concurrent pharmacological- and immunological tissue labeling can facilitate the investigation of molecular pharmacological interactions within a well-defined anatomical context.

Considering the D_3R preference of FLuo-CAR in the IoC, we visualized the distribution of drug binding sites together with functionally related dopaminergic signaling proteins. Firstly, we selected dopamine- and cAMP-regulated neuronal phosphoprotein of molecular weight 32,000 (DARPP-32) as a concomitant target, which represents a key intracellular modulator of dopaminergic signaling in striatal medium spiny neurons. Accordingly, DARPP-32 immunostaining showed the prominent

expression of the protein throughout the whole striatum (Fig. 5a). On the other hand, it was below detection sensitivity in the IoC on large scale confocal microscopic images. Another characteristic feature of the striatum is its intense dopaminergic innervation. Therefore, we next performed anti-tyrosine hydroxylase (TH) immunolabeling, which visualizes the key neurotransmitter synthesizing enzyme in dopaminergic afferents. In contrast to DARPP-32, TH-immunoreactive afferents constitute an extensive meshwork in the granular as well in the hilar subregions of the islands (Fig. 5b). Since our regional analysis showed that the dense aggregation of Fluo-CAR binding sites matches with sites of local dopamine synthesis, we next applied super-resolution microscopy to investigate the more precise anatomical organization of Fluo-CAR targets and TH-immunopositive terminals. We performed combined confocal and PharmacoSTORM imaging of TH immunostaining and Fluo-CAR binding sites (Fig. 5c,d). Surprisingly, in contrast to our low magnification images, Fluo-CAR LPs rather avoided the TH-immunolabeled dopaminergic terminals at the nanoscale level. These results highlight that the distribution of drug binding sites needs to be analyzed at multiple scales to be able to draw functionally relevant conclusions from anatomical observations.

DOI:10.14753/SE.2022.2679

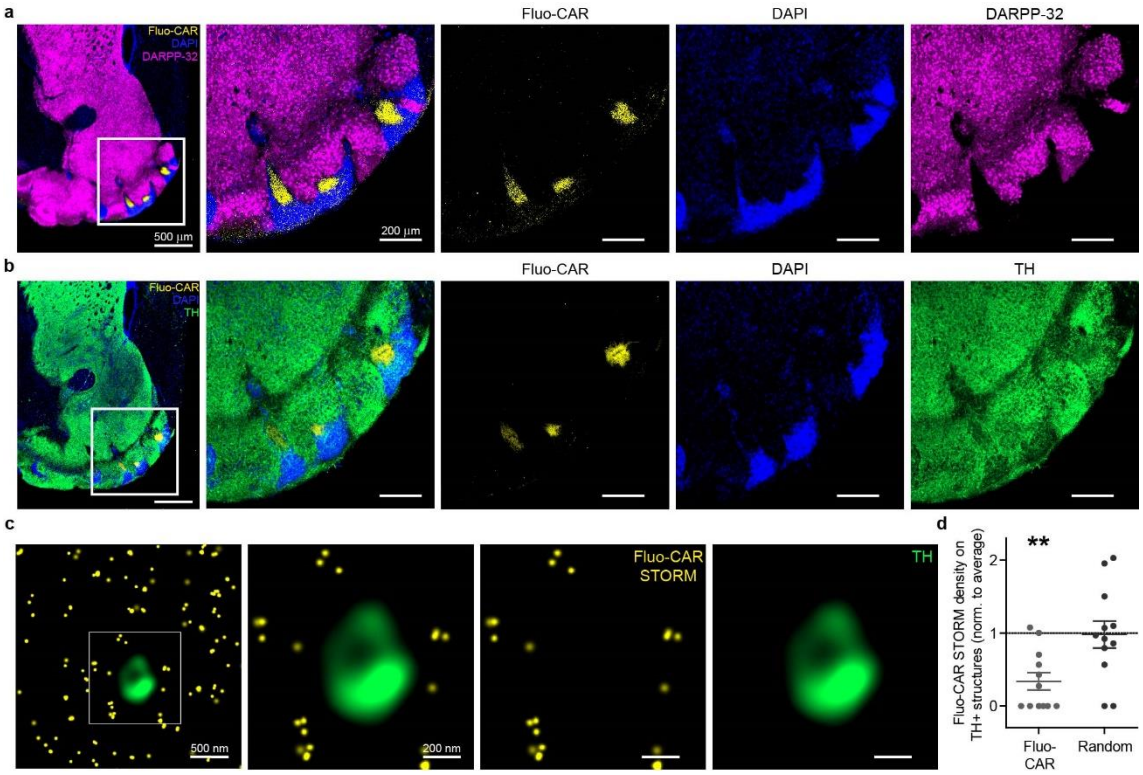

Figure 5. Correlated imaging of Fluo-CAR binding sites with immunolabeled dopaminergic signaling proteins. ***(a-b)*** *Representative images of combined Fluo-CAR labeling and immunolabeling in the mouse basal forebrain. Acute slices were incubated with 300 nM Fluo-CAR and were further processed for immunostaining against well-known dopaminergic signaling proteins.* ***(a)*** *Comparative analysis of Fluo-CAR and DARPP-32 distributions reveals the lack of DARPP-32 labeling in the cell bodies of IoC granule cells and in the hilar subregion.* ***(b)*** *In contrast to DARPP-32**,** a dense TH immunopositive meshwork of neuronal processes was found throughout the IoC, indicating the aminergic innervation of this region.* ***(c)*** *High-power confocal images of TH immunopositive boutons correlated with Fluo-CAR-based PharmacoSTORM localization point pattern. High-density Fluo-CAR binding sites avoid TH+ afferents.* ***(d)*** *Quantitative analysis of the spatial relation between Fluo-CAR binding sites and dopaminergic afferents in the IoC. If TH+ terminals would be the subcellular structures that underly the prominent Fluo-CAR labeling in the IoC, we would expect an accumulation of the PharmacoSTORM signal on them. However, we found that the density of Fluo-CAR LPs on TH+ compartments was less than it would be expected from a random distribution of the same number of LPs. (Data are normalized to the Fluo-CAR STORM LP density on each image, thus the hypothetical average density equals 1.)*

Wilcoxon signed rank test was used to test if data are statistically different from 1 (n = 12, data are from 5 animals). Fluo-CAR density is significantly smaller on dopaminergic terminals (P = 0.0048) for real Fluo-CAR binding sites, but P = 0.7836 if PharmacoSTORM LPs are spatially randomized.

3.2.4. Cell-type specific PharmacoSTORM imaging

Centrally acting drugs can modulate multiple parallel brain circuits that are formed by a large number of anatomically and functionally diverse neuronal cell types. Accordingly, it is becoming increasingly appreciated that cell-type-specific approaches are required to gain insights into the neurobiological mechanisms of the pharmacological actions. To address this challenge, we further improved PharmacoSTORM to determine the cell-type specific binding sites of cariprazine within the Islands of Calleja circuitry. We exploited the possibility of multi-channel fluorescence imaging with pharmacological probes and developed a novel methodical procedure that enables the concurrent visualization of drug binding sites and individual neurons. To this end, IoC granule cells were functionally characterized by whole-cell patch-clamp electrophysiological recordings in acute brain slices. Thereafter, cells were filled with biocytin via the patch pipette, and then the preparations were treated with Fluo-CAR (Fig. 6). This way, we were able to perform correlated three-dimensional analysis of granule cell morphology with Fluo-CAR distribution by multi-channel confocal microscopy. Our systematic analyses revealed that a thin, gracile process, which shows morphological features of an axon, consistently enters the Fluo-CAR rich hilus and arborizes exclusively in this subregion. On the other hand, dendrite-like processes of granule cells and their branches remain confined in the cell-dense area.

Our differential observations at different anatomical scales with dopaminergic terminals encouraged us to deeper analyze the spatial relation between the drug binding sites and neuronal processes of morphologically- and electrophysiologically-characterized granule cells (Fig. 7.) We performed correlated confocal and PharmacoSTORM imaging of granule cell axons and Fluo-CAR respectively (Fig. 7f-j). In contrast to the nanoscale mismatch between dopaminergic terminals and PharmacoSTORM LPs, Fluo-CAR binding sites were preferentially located at granule

cell axons. The nanoscale association could be observed both on the axon varicosities and on inter-connecting axonal segments, and we found no significant difference between the PharmacoSTORM LP densities on these subcellular compartments (Fig. 7 h-j).

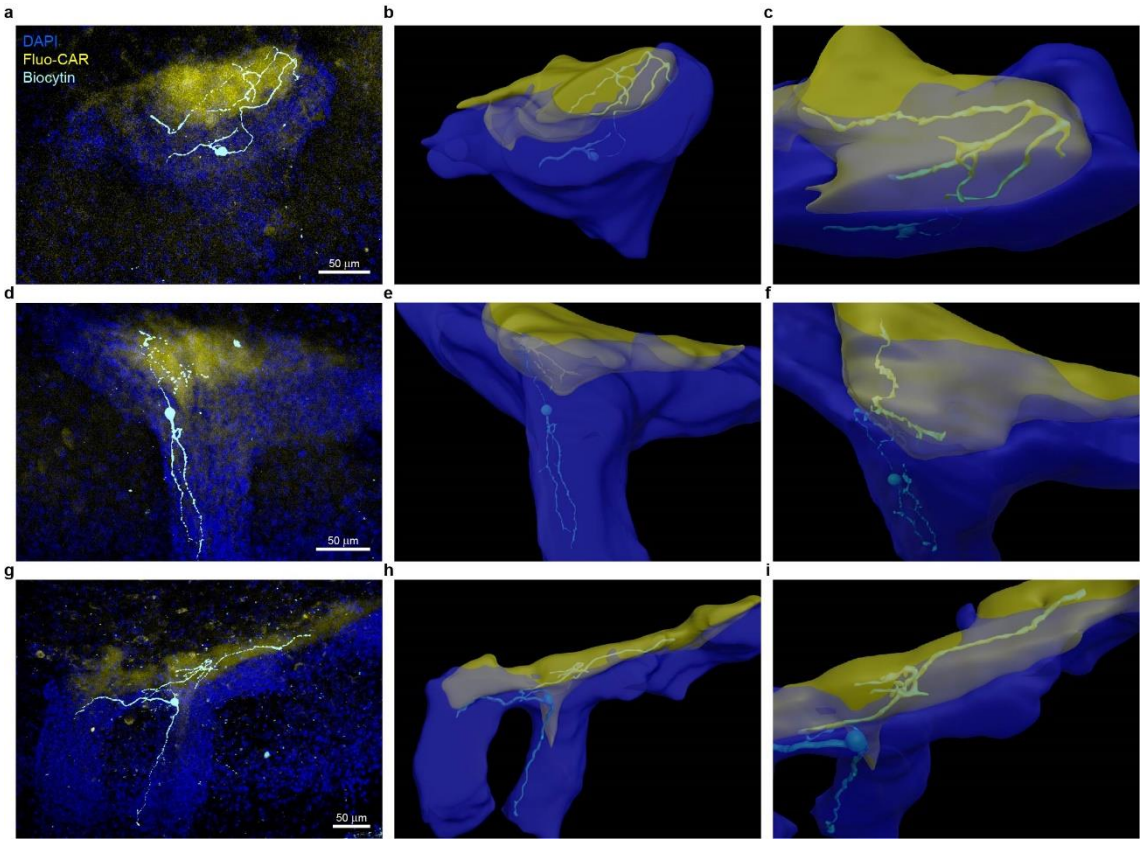

Figure 6. Correlated three-dimensional analysis of neuronal morphology and Fluo-CAR binding in the IoC. (a,d,g) *Maximum intensity projections of confocal microscopic z-stacks of mouse coronal slices, labeled with Fluo-CAR and DAPI. In the same sections, IoC granule cells were filled with biocytin and visualized by fluorescent streptavidin. A common morphological feature of granule cells is that the main processes specifically arborize within the IoC: the thick, dendrite-like processes remain restricted to the cell-dense region, and the thin, axon-like processes exclusively target the Fluo-CAR rich hilus.* ***(b,e,h)*** *3D models of granule cells (cyan) and high-density Fluo-CAR binding sites (yellow) based on confocal microscopic z-stacks. The cell-dense region of the IoC (blue) and the Fluo-CAR rich hilus are transparent for the better visualization of granule cell neurites.* ***(c,f,i)*** *Higher-magnification top angle view of the 3D models from (b,e,h) highlight the morphology of „hilar" processes of granule cells.*

DOI:10.14753/SE.2022.2679

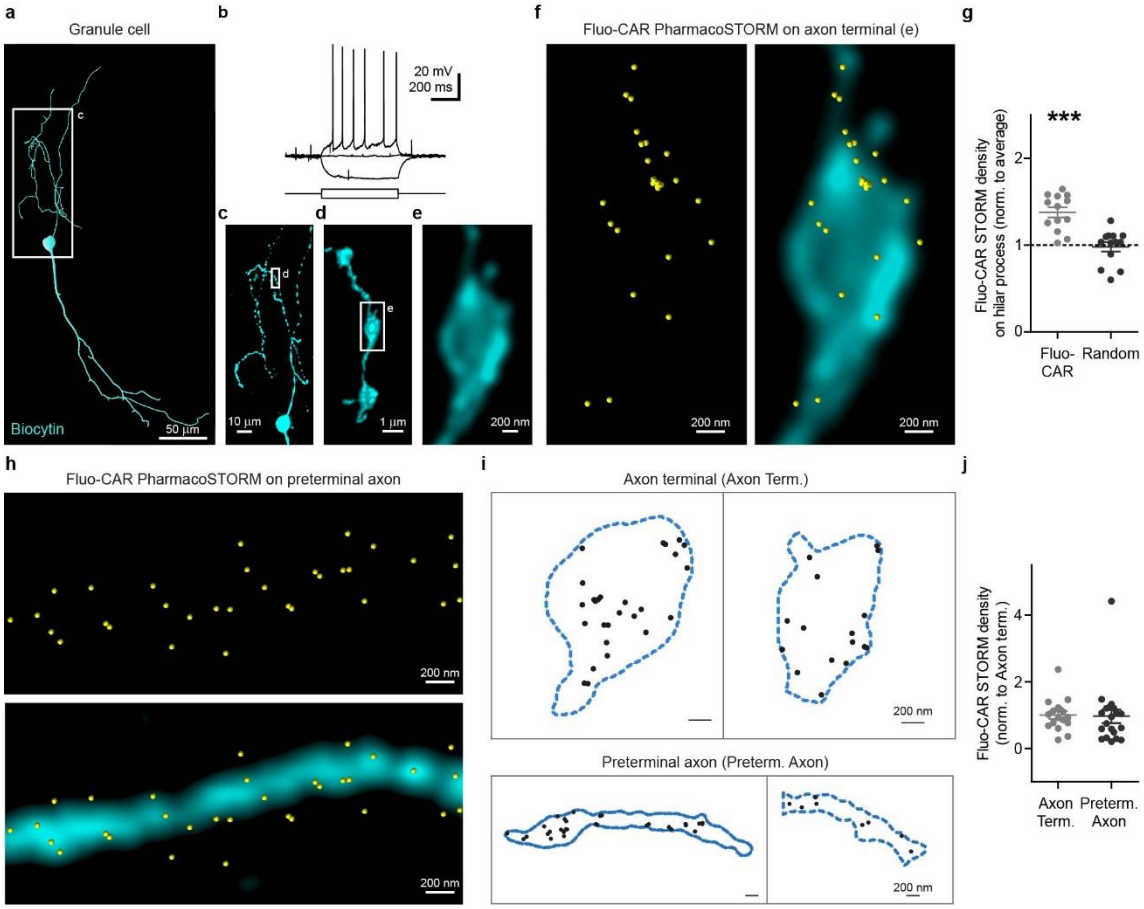

Figure 7. Cell-type-specific analysis of Fluo-CAR binding. ***(a,b)*** *A representative granule cell in the Island of Calleja was filled with biocytin during whole-cell patch-clamp recordings in acute coronal slices. The same sections were live-stained with 300 nM Fluo-CAR for the combined visualization of drug binding sites and 3D neuronal morphology. Note that the arborization of the granule cell strictly follows the unique shape of the Island of Calleja, and one of its processes preferentially branches in the hilar region.* ***(b)*** *3D reconstruction of the same granule cell. The neuronal process that enters the Fluo-CAR-rich region is marked in yellow, and hereinafter referred to as hilar process.* ***(c-h)*** *Visualization of Fluo-CAR drug binding sites on an anatomically- and electrophysiologically-characterized neuron. To decipher morphological (c) as well as functional (d) characteristic of individual cells, neurons were filled with biocytin during whole-cell patch-clamp recordings.* ***(c)*** *Representation of an IoC granule cell, reconstructed with Neurolucida neuron tracing software.* ***(d)*** *Voltage traces in response to +7 pA, 0 pA, -10 pA depolarizing and hyperpolarizing current steps from resting membrane potential recorded.* ***(c-e)*** *Multi-scale visualization of the hilar process.* ***(c)*** *Overall morphology of the neurite is represented by a maximum intensity z-projection of*

a low-magnification confocal image stack. ***(d)*** *Volume view of a high-resolution confocal image stack of a varicose segment. High magnification deconvolved confocal image of an individual granule cell bouton (e).* ***(f)*** *Fluo-CAR binding sites on the varicosity from (e) were investigated by correlated confocal and PharmacoSTORM imaging.* ***(g)*** *Statistical investigation of Fluo-CAR enrichment on granule cell varicosities. Scatter dot plot shows the PharmacoSTORM LP density on hilar processes normalized to the average LP density on each image. Wilcoxon signed rank test reveals that Fluo-CAR density on the hilar processes of biocytin-filled cells is significantly above the average of 1 (n = 13, data are from 6 animals, P = 0.0002). As a control, we randomly distributed the same number of LPs, in which case LP density values on the hilar processes were not different from 1 (P = 0.8394).* ***(h)*** *Correlated confocal and PharmacoSTORM image of a long preterminal segment of a biocytin-filled granule cell axon (cyan).* ***(i)*** *Schematic illustration of segmented PharmacoSTORM images of axon terminals (Axon Term.) and preterminal axonal (Preterm. Axon) segments. The contours of distinct axonal subcompartments were determined by correlated high-resolution confocal microscopic images (shown with blue dashed lines). Fluo-CAR-based PharmacoSTORM LPs are presented by black dots.* ***(j)*** *Scatter dot plot represents the Fluo-CAR LP density on different subcompartments of granule cell axons. Data are normalized to the mean LP density on axon terminals. Two-tailed Mann-Whitney test revealed that the density of Fluo-CAR binding sites is not significantly different on axon terminals and preterminal axon segments (n = 17 and n = 20, respectively, P = 0.402).*

3.2.5. PharmacoSTORM can reveal real *in vivo* binding sites of cariprazine

Finally, we raised the question whether the *in vitro* nanoscale distribution of Fluo-CAR PharmacoSTORM LPs reflects real *in vivo* binding sites of the original clinical drug. According to our previous competitive PharmacoSTORM-based assay, cariprazine occupies the same binding sites as Fluo-CAR if it is applied to *in vitro* acute brain slices, it. As a next step we directly tested whether the nanoscale localization of cariprazine in the brain of live mice can be determined by the displacement of its fluorescent analog. To this end, we intraperitoneally injected cariprazine to live mice 2 hours before pharmacological labeling and subsequently performed confocal and STORM imaging

(Fig. 8a). *In vivo* cariprazine administration prevented Fluo-CAR binding in the hilus of the IoC, and PharmacoSTORM LPs were fully eliminated (Fig. 8b). Furthermore, we applied correlated confocal and PharmacoSTORM imaging of dopaminergic boutons and Fluo-CAR to further demonstrate how super-resolution imaging with fluorescent pharmacoprobes can bring quantitative pharmacology and precise anatomical studies together (Fig. 8c-e).

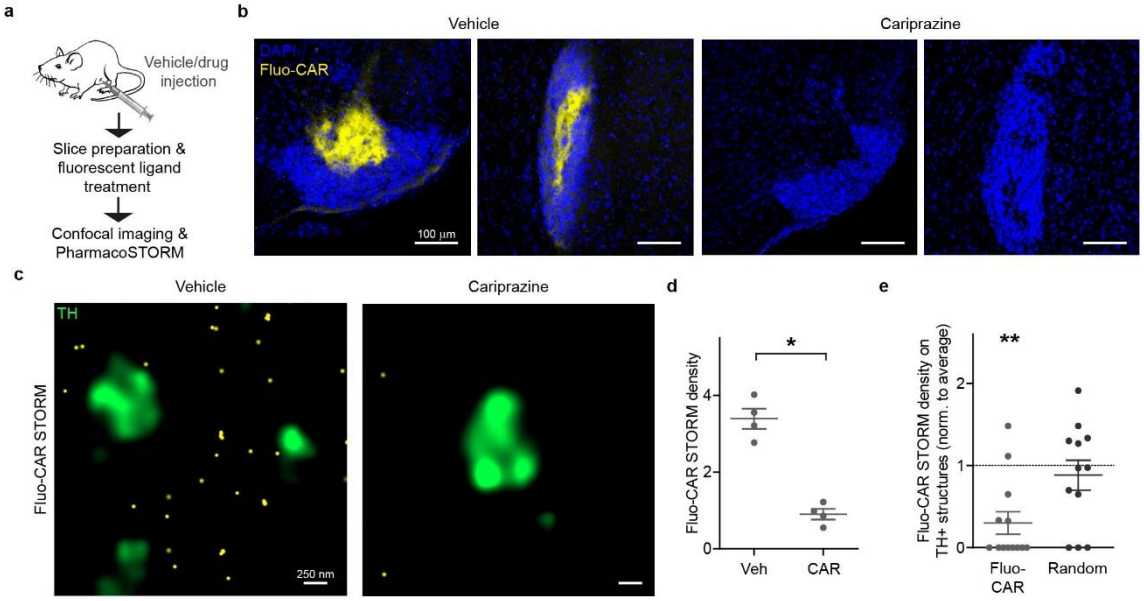

Figure 8. Deciphering in vivo target engagement of cariprazine by PharmacoSTORM. ***(a)*** *Schematic illustration of the competitive binding assay. 1 mg/kg cariprazine or vehicle was intraperitoneally injected to live animals, two-hours before the pharmacological staining procedure with 30 nM Fluo-CAR.* ***(b)*** *Confocal images of the rostromedial extension of the IoC (left) and the so-called major island (right) show that in vivo administered cariprazine efficiently prevented Fluo-CAR binding in the hilus of the IoC.* ***(c)*** *Analysis of the competitive ligand binding experiment in an anatomical context by correlated confocal and quantitative PharmacoSTORM imaging. In vehicle treated animals, Fluo-CAR LPs are abundant in the hilus of the IoC but not associated to TH+ terminals. On the other hand, cariprazine administration markedly decreased the number of Fluo-CAR binding sites, indicating that the PharmacoSTORM LPs illuminate in vivo molecular targets of the original antipsychotic.* ***(d)*** *Statistical analysis of the Fluo-CAR binding site density (LPs/µm^2) in the hilus of the IoC in cariprazine- or vehicle-treated mice (n = 4). The average density of PharmacoSTORM LPs obtained throughout the IoC of each mouse is plotted. Two-tailed Mann-Whitney test was performed to test if Fluo-*

CAR density values are significantly different (n=4, P = 0.0286). Data are presented as mean ± S.E.M.

4. Discussion

Labeled analogues of GPCR ligands are instrumental to study the physiology and pharmacology of receptors. Since their first applications in the 1970s, radioligand-based assays represent the gold-standard methods to characterize drug-target interactions. On the other hand, due to the rapid spread of fluorescence techniques and the general safety concerns with radioactive materials, fluorescent drugs have become popular alternatives to their radioactive counterparts in ligand binding measurements[9]. Furthermore, they offer the possibility to answer emerging questions about GPCRs that are hard or impossible to address with classical radioassays.

4.1. Availability and development of labeled GPCR ligands

In my doctoral thesis, I introduced two novel techniques that exploit the potential of fluorescently labeled small molecules and studied different aspects of DR ligand-binding. A key objective during the development of the new methods was to design workflows that can be readily applied to a variety of other fluorescent ligand-GPCR pairs. Certainly, the generalization of our advanced methodologies requires the broad availability of appropriate fluorescently labeled drugs. The basic concept behind the development of radioactive or fluorescent drugs is to chemically modify already known, well-characterized receptor ligands without causing major alterations in their receptor binding profiles. In the case of tritiated radioligands, the exchange of a hydrogen atom to a radioactive ^{3}H scarcely effects the overall molecular structure[66]. Also, with a few exceptions, a ^{125}I isotope can be introduced to iodinated drugs without dramatic changes in their receptor affinity[67]. Conversely, the production of fluorescent small molecules that possess the original characteristics of the unlabeled compounds is more challenging, because the conjugation of relatively large fluorescent moieties might have greater influence on receptor-ligand interactions than the incorporation of radioisotopes. On the other hand, the rapidly progressing field of GPCR structural biology coupled with advanced chemical methodologies provide considerable assistance to overcome this difficulty[54–56]. The number of available GPCR structures in different conformational states is rapidly rising due to the advanced X-ray crystallographic techniques and to the recent breakthrough methodology of electron cryo-microscopy[57]. Furthermore, the

DOI:10.14753/SE.2022.2679

expanding set of structures is acquainted by advanced computational approaches to simulate and predict the docking of millions of small molecules. We applied a commercially available fluorescent D_1 receptor ligand, and also provided an example of how recent technical improvements in the field of structural biology can facilitate the rational design of optimal pharmacological probes (or pharmacoprobes in short) by the development of a Sulfo-Cy5-tagged analogue of an antipsychotic drug, cariprazine (Fluo-CAR) (Fig. 9a-d).

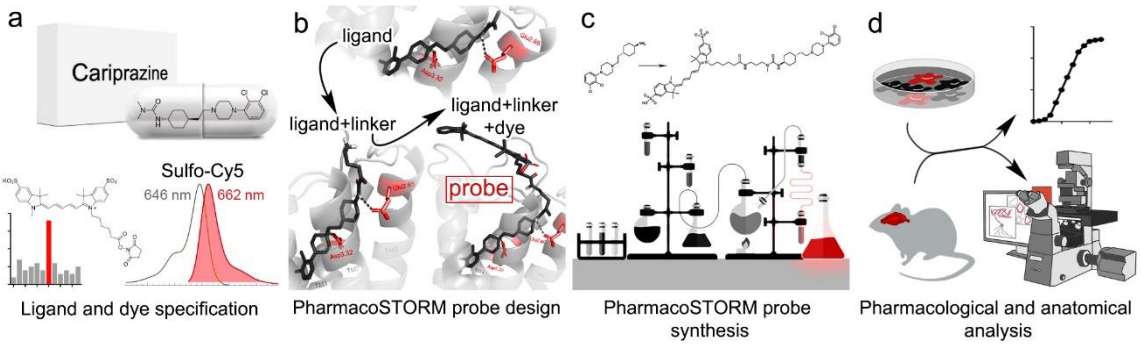

Figure 9. General workflow for the development and applications of novel PharmacoSTORM probes

The novel fluorescent probe displayed highly similar pharmacological characteristics as the original drug, and the fluorophore preserved its excellent photochemical properties for microscopic imaging. Notably, the synthesis and application of radioactive isotopes require a strict regulatory framework, however the development of fluorescent ligands does not necessitate such security measures[12]. Another benefit of fluorescent tagging is that numerous fluorophores with different excitation wavelength, brightness, and water-solubility are readily available, and thus can accomplish the objective of various fluorescence-based experiments.

4.2. Importance of easily reachable fluorescent ligand binding assays

Considering the expanding knowledge of receptor-ligand interactions, the number of commercially available or custom-made fluorescent ligands is expected to rapidly increase in the future. Therefore, it is of growing importance to develop simple, easily

accessible fluorescent ligand-based binding assays that can be generalized for a broad range of receptors. Here, we took advantage of a commercially available fluorescent D_1R receptor antagonist to quantify the ligand binding of D_1 dopamine receptors with a novel BRET-based approach. Previous BRET-based measurements of dopamine receptor occupancy with fluorescent pharmacoprobes required the covalent modification of the receptors[15]. In this study, we successfully assessed the small molecule binding of unmodified D_1Rs in the plasma membrane of live HEK 293 cells with a novel Gaussia-luciferase biosensor and a fluorescent D_1R antagonist. Due to the excellent luminescent characteristics of the Gaussia-luciferase enzyme, the high signal-to-noise ratio and the simple execution of the measurements, our assay may also be suitable for high-throughput D_1R ligand screening.

The same ligand (BODIPY-FL-SKF-83566) has been previously applied for the characterization of non-labeled D_1R ligands in a fluorescence anisotropy-based assay[52]. Fluorescence anisotropy-based ligand binding measurements are also relatively easy to perform, however they do not allow ratiometric measurements and they require very high receptor concentrations that cannot be achieved in routine heterologous expression systems. One way to solve this issue, is to express GPCRs on the surface of budding baculoviruses[52, 68]. However, the easy pharmacological manipulation of routine expression systems, such as HEK 293 cells, and the simple co-expression of intracellular signaling molecules that can shift GPCRs between different affinity states offer more opportunities to investigate complex pharmacological phenomena[69–71].

4.3. Pharmacoprobes as microscopic labeling tools

4.3.1. General aspects of pharmacoprobe-based tissue labeling

In addition to their various applications in binding assays, fluorescently labeled drugs have also been visualized by various optical microscopic modalities in cell cultures and tissue specimen [72–79]. A general advantage of pharmacoprobe-based receptor labeling techniques is that small molecules can readily penetrate thick tissue samples and provide a homogenous binding pattern. On the other hand, the most frequently applied labeling technique for microscopic imaging is immunostaining, which usually requires the

permeabilization of chemically-fixed samples before the labeling procedure to enhance the tissue penetration of relatively large-size antibodies. Even if permeabilization steps are included in the sample handling protocol, immunolabeling may take considerable time (days), and antigens in crowded molecular complexes may remain inaccessible to antibodies. In addition, heavy permeabilization methods can substantially alter the ultrastructure of the tissue. Therefore, the rapidly progressing field of deep tissue fluorescence microscopy and volumetric super-resolution imaging[80–83] can greatly profit from novel small molecular weight probes. In this study, with the help of Fluo-CAR, we successfully labeled D_3Rs within live acute brain slices that were substantially thicker (from hundreds of μm to the mm range) than tissue sections generally used for immunostaining (20-60 μm).

Furthermore, we established an experimental workflow to combine pharmacoprobe- and antibody-based labeling for the simultaneous visualization of drug binding sites and anatomical marker proteins. Certainly, due to the additional washing steps, only high-affinity fluorescent ligands with long receptor residence time are suitable for the combined pharmacological and immunostaining of target proteins. In general, if rapidly dissociating fluorescent ligands are used for receptor localization studies, only fast and delicate post-processing steps can be performed on the sample before microscopic imaging to acquire a sufficient level of fluorescence signal. Moreover, in the case of multi-target fluorescent ligands, differences in the dissociation rate constants at distinct receptors must be taken into consideration if the experiments attempt to compare the level of target occupation at different receptor subtypes. It is conceivable that the expanding set of covalent GPCR ligands will overcome these constraints by providing guidance for the synthesis of novel fluorescent pharmacoprobes that can irreversibly attach to their receptors. Covalent GPCR ligands have been designed for a variety of purposes by numerous different technical approaches[84, 85]. Irreversibly binding dopamine receptor ligands have been introduced for D_1 and D_2-like receptors as well. However, in many cases, the covalent attachment of these probes necessitates incorporation of receptor mutations, which complicates their adaptation to tissue samples[86–88].

Importantly, as is the case with all experimental techniques, pharmacoprobe-based labeling requires strict validation steps. A great advantage of labeled drugs is that the

specificity of their tissue localization pattern can be readily tested in competition ligand binding assays. In contrast, the selectivity of a novel antibody has to be verified on samples from knockout animals, which can substantially increase the costs of the experiments or might even be unavailable[89]. The generally high batch-to-batch variability further challenges the quality control of experimental antibodies [90, 91]. In addition, regularly applied fluorescent secondary antibodies hold variable number of fluorophores, which may result in the false detection of "artificial clusters" in SMLM studies and may easily lead to the overcounting of the receptor targets without rigorous validation. In this regard, rationally designed fluorescent drugs may be particularly advantageous for quantitative super-resolution pharmacological receptor studies. As opposed to the unpredictable amplification steps during immunolabeling, fluorescent ligands bind their targets with known stoichiometry and carry a single fluorophore.

4.3.2. Pharmacoprobes for anatomical localization studies

Although fluorescent ligands provide a straightforward opportunity to decipher the anatomical localization of their high-affinity receptor partners in complex tissue preparations, the precise mapping of a specific receptor subtype requires a selective pharmacoprobe, which might be hard to acquire if structurally homologous receptors are also expressed in the same sample. This applied to D_3Rs since it shares fundamental structural similarities with other members of the D_2-like dopamine receptor subfamily[92, 93]. The primary orthosteric ligand binding pockets of D_2 and D_3 receptors are principally formed by the same conserved amino acid residues, and the region-specific expression profiles of the two receptor subtypes are greatly overlapping in many brain areas[28]. Despite of the remarkable structural homology between the two receptor subtypes, several D_3R-preferring labeled ligands have been successfully developed and have been applied for a variety of studies. However most of them has only moderate D_3R selectivity, which complicates their interpretation. These include radiotracers for *in vivo* positron emission tomography imaging and radioligands for autoradiography[35, 51, 94, 95]. Recently, a new set of D_3R-selective fluorescent ligands have been developed and thoroughly characterized in signaling assays. Although their performance have not been shown in tissue samples yet, they may also have the remarkable potential to further investigate the

high-precision anatomical localization of this receptor subtype[15, 50]. Furthermore, the recently resolved structures of D_2 and D_3 receptors will likely facilitate the development of additional selective high-affinity DR probes[93, 96].

4.3.3. Microscopic pharmacoprobes based on clinically applied drugs

Labeled therapeutics can be excellent tools for the anatomical investigation of their high-affinity molecular targets. However, their unique power is their ability to visualize the distribution of *in vivo* administered pharmacoprobes and thus provide important information about their pharmacodynamic and pharmacokinetic actions. Nonetheless, the investigation of labeled probes in brain tissue after systemic exposure is an extraordinary challenge, since the blood-brain barrier greatly determines the chemical properties of molecules that can enter the CNS. Certainly, the introduction of a single radioisotope to a neuropsychiatric drug has less impact on its ability to cross the blood-brain barrier than the fusion of a relatively large fluorescent moiety. In *ex vivo* autoradiography experiments, radioactive drugs are administered *in vivo*, then animals are sacrificed, and the distribution of the pharmacoprobes is analyzed on thin tissue sections[97]. However, the relatively low resolution and the lack of additional anatomical markers on classical autoradiographs do not allow the visualization of the precise binding sites within distinct brain regions and on the surface of specific cell types. Contrarily, super-resolution multi-color fluorescence microscopy allows the nanoscale spatial localization of proteins on specified anatomical structures. To circumvent the limitations of the blood-brain barrier and to determine the *in vivo* sites of cariprazine action with the help of a fluorescent analogue, we established a displacement assay in which unmodified cariprazine was administered to live mice, then Fluo-CAR treatment was executed on acute brain slices. In this manner, the displacement of the fluorescent signal in cariprazine-treated animals demonstrated that our *in vitro* PharmacoSTORM experiments detect real *in vivo* binding sites of the antipsychotic drug. Importantly, a single fluorescent ligand with a well-defined binding pattern can reveal *in vivo* binding sites of any other small molecules that occupy the same targets. Furthermore, competitive fluorescent-ligand binding experiments can also uncover unexpected off-target binding sites that may underlie clinical side effects. In this regard, fluorescent D_3R probes are likely to be of outstanding

pharmaceutical interest, since D_3R has been recently recognized as an *in vitro* target of certain drug excipients, but their D_3R engagement in brain tissue after systemic administration remained elusive[36].

4.4. Multi-scale anatomical distribution of fluorescent cariprazine – significance of Islands of Calleja granule cells

As we demonstrated by the mapping of Fluo-CAR binding sites in mouse brain tissue, a key strength of the PharmacoSTORM approach is that it supports the analyses of pharmacological interactions at multiple anatomical levels. The region-specific distribution of the novel fluorescent derivative was consistent with the D_3R preference of the original drug, and the most prominent signal was detected in the Islands of Calleja, where high levels of D_3R expression have been previously shown by low-resolution mRNA *in situ* hybridization and autoradiographic studies[43, 98, 99]. Importantly, the presence of D_3Rs at lower density has been shown in several other brain regions as well[99–104], however, the prominent Fluo-CAR binding clearly demarcated the IoC from neighboring striatopallidal regions. Moreover, the three-dimensional (3D) reconstruction of high-density ligand binding sites discerned that the IoC represents a surprisingly large continuous neuronal assembly. The complex forms several inclusions in the olfactory tubercle (often referred to as minor islands), and the so-called major island is elongated at the medial border of the nucleus accumbens. Fluo-CAR binding sites disappeared from all parts of the IoC of D_3R KO animals, suggesting that this receptor subtype is the main molecular target throughout the whole complex. By relying on the high resolution of STORM imaging, we have shown that the nanoscale distribution of drug binding sites is not associated with dopaminergic axon terminals, suggesting that the majority of D_3Rs in the IoC are regulated by volume transmission. Our findings are in agreement with the high affinity of D_3Rs towards its endogenous ligand, dopamine: D_3R has 100-fold higher affinity to dopamine than D_2R[93], and thus can be efficiently activated at low ligand concentrations, far from the dopamine release sites. Altogether, these results implicate that the concerted modulation of D_3Rs in the IoC may underly important behavioral effects of cariprazine. Despite of the strategic localization of the IoC complex, and the widely accepted role of D_3R in various mental illnesses[43, 104–106],

the contribution of IoC granule cells to the pathophysiology or pharmacology of neuropsychiatric diseases has not been experimentally investigated before. Here, we showed by cell-type- and compartment-specific PharmacoSTORM imaging that cariprazine preferentially targets IoC granule cell axons, and thus modulate their neuronal output. As a partial agonist[42], cariprazine may activate D_3R signaling at low dopamine levels but can also antagonize the effects of high neurotransmitter concentrations. Consequently, its agonistic or antagonistic actions may alternate with the fluctuations of the extracellular dopamine level, that reflect different internal states of the brain and are coupled with changes in outward behavior[29].

DOI:10.14753/SE.2022.2679

5. Conclusions

In the current thesis, I presented two novel methods that exploit fluorescent drugs for studying receptor-ligand interactions and demonstrated their usefulness by the examination of dopamine receptor targeting drugs.

First, we showed that the novel Gaussia-luciferase-based plasma membrane-targeted biosensor is an excellent tool for the precise characterization of D_1R ligand binding. We found the following advantages of the assay: 1. ligand binding of unmodified D_1Rs can be readily studied in a convenient assay format; 2. specific bystander BRET can be detected with high signal-to-noise ratio; 3. the measurement is cost-efficient, since it required a relatively non-expensive luciferase substrate, coelenterazine.

Second, we proposed a novel fluorescent ligand-based framework, called PharmacoSTORM. To corroborate the clinical significance of our work, we introduced our workflow by the investigation of a blockbuster antipsychotic drug, cariprazine, and reached the following conclusions: 1. The development of a fluorescent cariprazine analogue (Fluo-CAR) demonstrates that the generation of specific pharmacological probes can be greatly facilitated by structure-based rational design and advanced chemical techniques. Fluo-CAR preserved the main pharmacological characteristics of the original drug and its high affinity towards D_3R made it a suitable labeling probe for this receptor subtype in both overexpression and native systems for super-resolution as well as conventional fluorescence microscopy. 2. We provided a multi-scale anatomical map of Fluo-CAR binding sites in the mouse forebrain, which revealed extensive D_3R labeling in the Islands of Calleja (IoC). Detailed 3D analysis of the unique Fluo-CAR binding pattern revealed that the IoC represent a large, continuous assembly of granule cells. 3. We introduced a straightforward experimental way to study the nanoscale distribution of unlabeled drugs in the mouse brain and verified that Fluo-CAR binding sites in the IoC represent real *in vivo* targets of cariprazine. 4. We showed that pharmacoprobes can be combined with immunohistochemical markers. Moreover, we proved the feasibility of cell-type-specific PharmacoSTORM imaging on electrophysiologically- and morphologically-characterized neurons. We revealed Fluo-CAR binding sites on DARPP-32 negative granule cell axons in the Islands of Calleja, that were surrounded by tyrosine hydroxylase-positive dopaminergic nerve terminals.

DOI:10.14753/SE.2022.2679

Taken together, our data implicate that PharmacoSTORM has outstanding power to visualize receptor binding of individual drug molecules in a native tissue environment.

DOI:10.14753/SE.2022.2679

6. Summary

Fluorescent ligands are emerging tools for the characterization and microscopic visualization of receptor-ligand interactions. In this thesis, I briefly review the key concepts of fluorescent ligand-based GPCR assays and introduce two novel methodical developments. I demonstrate their advantages by the investigation of dopamine receptors.

Firstly, we applied a novel BRET assay to assess the ligand binding of the D_1 dopamine receptor. An important advance of our approach is that the assay requires no genetic modification of the receptor of interest, since BRET is measured between a cell surface-anchored Gaussia-luciferase and fluorescent ligands bound to native receptors. We adjusted the approach for D_1R using a commercially available fluorescent D_1R ligand and showed that the assay is suitable for competitive ligand binding measurements.

In the second part, we established a novel framework, termed PharmacoSTORM, that enables precise anatomical localization of identified drug binding sites. We designed and synthesized a novel fluorescent probe based on the D_3R-preferring antipsychotic drug, cariprazine. We demonstrated that the fluorescent analog (Fluo-CAR) displays similar pharmacological characteristics as the original drug and is amenable for a variety of fluorescence imaging techniques, including STORM super-resolution microscopy. 3D anatomical mapping of Fluo-CAR distribution in the mouse brain showed the highest density of Fluo-CAR binding sites in the Islands of Calleja (IoC) and revealed that this enigmatic brain region represents a large continuous network of granule cells in the tubular striatum. PharmacoSTORM super-resolution imaging uncovered that at the nanoscale level, Fluo-CAR interacted with D_3Rs on granule cell axons. Combined pharmacological- and immunological labeling revealed that Fluo-CAR bound D_3Rs are not associated with dopaminergic terminals in the IoC, suggesting that they are mostly involved in dopaminergic volume transmission. Pharmacological and genetic control experiments confirmed that D_3Rs on granule cell axons represent real *in vivo* targets of the unmodified, clinically applied drug.

Taken together, these technical achievements show the power of fluorescent ligands for the high-resolution analyses of drug binding. Additionally, the prominent density of cariprazine binding sites on IoC granule cells implicates their importance in neuropsychiatric diseases and highlights their potential as future pharmacological targets.

7. References

1. Santos R, Ursu O, Gaulton A, Bento AP, Donadi RS, Bologa CG, Karlsson A, Al-Lazikani B, Hersey A, Oprea TI, Overington JP. (2017) A comprehensive map of molecular drug targets. *Nat. Rev. Drug Discov.*, **16**, 19–34.
2. Yang D, Zhou Q, Labroska V, Qin S, Darbalaei S, Wu Y, Yuliantie E, Xie L, Tao H, Cheng J, Liu Q, Zhao S, Shui W, Jiang Y, Wang MW. (2021) G protein-coupled receptors: structure- and function-based drug discovery. *Signal Transduct. Target. Ther.*, **6**, 7.
3. Hulme EC, Trevethick MA. (2010) Ligand binding assays at equilibrium: validation and interpretation. *Br. J. Pharmacol.*, **161**, 1219.
4. Flanagan CA. (2016) GPCR-radioligand binding assays. *Methods Cell Biol.*, **132**, 191–215.
5. Carletti R, Tacconi S, Mugnaini M, Gerrard P. (2017) Receptor distribution studies. *Curr. Opin. Pharmacol.*, **35**, 94–100.
6. Griem-Krey N, Klein AB, Herth M, Wellendorph P. (2019) Autoradiography as a Simple and Powerful Method for Visualization and Characterization of Pharmacological Targets. *J. Vis. Exp.*, **145**, 1–11.
7. Carpenter JW, Laethem C, Hubbard FR, Eckols TK, Baez M, McClure D, Nelson DL, Johnston PA. (2002) Configuring Radioligand Receptor Binding Assays for HTS Using Scintillation Proximity Assay Technology. *Methods Mol. Biol.*, **190**, 31–49.
8. Zhang R, Xie X. (2012) Tools for GPCR drug discovery. *Acta Pharmacol. Sin.*, **33**, 372.
9. Soave M, Briddon SJ, Hill SJ, Stoddart LA. (2020) Fluorescent ligands: Bringing light to emerging GPCR paradigms. *Br. J. Pharmacol.*, **177**, 978–991.
10. Stoddart LA, White CW, Nguyen K, Hill SJ, Pfleger KDG. (2016) Fluorescence- and bioluminescence-based approaches to study GPCR ligand binding. *Br. J. Pharmacol.*, **173**, 3028.
11. Ciruela F, Jacobson KA, Fernández-Dueñas V. (2014) Portraying G Protein-Coupled Receptors with Fluorescent Ligands. *ACS Chem. Biol.*, **9**, 1918–1928.
12. Stoddart LA, Kilpatrick LE, Briddon SJ, Hill SJ. (2015) Probing the pharmacology

of G protein-coupled receptors with fluorescent ligands. *Neuropharmacology*, **98**, 48–57.

13. Pfleger KDG, Eidne KA. (2006) Illuminating insights into protein-protein interactions using bioluminescence resonance energy transfer (BRET). *Nat. Methods*, **3**, 165–174.
14. Stoddart LA, Johnstone EKM, Wheal AJ, Goulding J, Robers MB, Machleidt T, Wood K V., Hill SJ, Pfleger KDG. (2015) Application of BRET to monitor ligand binding to GPCRs. *Nat. Methods*, **12**, 661–663.
15. Allikalt A, Purkayastha N, Flad K, Schmidt MF, Tabor A, Gmeiner P, Hübner H, Weikert D. (2020) Fluorescent ligands for dopamine D2/D3 receptors. *Sci. Rep.*, **10**, 21842.
16. Emami-Nemini A, Roux T, Leblay M, Bourrier E, Lamarque L, Trinquet E, Lohse MJ. (2013) Time-resolved fluorescence ligand binding for G protein-coupled receptors. *Nat. Protoc.*, **8**, 1307–1320.
17. Stoddart LA, Kilpatrick LE, Hill SJ. (2018) NanoBRET Approaches to Study Ligand Binding to GPCRs and RTKs. *Trends Pharmacol. Sci.*, **39**, 136–147.
18. Wingler LM, McMahon C, Staus DP, Lefkowitz RJ, Kruse AC. (2019) Distinctive Activation Mechanism for Angiotensin Receptor Revealed by a Synthetic Nanobody. *Cell*, **176**, 479.
19. Al-Sabah S, Adi L, Bünemann M, Krasel C. (2020) The Effect of Cell Surface Expression and Linker Sequence on the Recruitment of Arrestin to the GIP Receptor. *Front. Pharmacol.*, **11**, 1271.
20. Huang B, Babcock H, Zhuang X. (2010) Breaking the Diffraction Barrier: Super-Resolution Imaging of Cells. *Cell*, **143**, 1047–1058.
21. Valli J, Garcia-Burgos A, Rooney LM, de Melo e Oliveira BV, Duncan RR, Rickman C. (2021) Seeing beyond the limit: A guide to choosing the right super-resolution microscopy technique. *J. Biol. Chem.*, **297**, 100791.
22. Dani A, Huang B, Bergan J, Dulac C, Zhuang X. (2010) Superresolution Imaging of Chemical Synapses in the Brain. *Neuron*, **68**, 843–856.
23. Dudok B, Barna L, Ledri M, Szabó SI, Szabadits E, Pintér B, Woodhams SG, Henstridge CM, Balla GY, Nyilas R, Varga C, Lee SH, Matolcsi M, Cervenak J, Kacskovics I, Watanabe M, Sagheddu C, Melis M, Pistis M, Soltesz I, Katona I.

(2015) Cell-specific STORM super-resolution imaging reveals nanoscale organization of cannabinoid signaling. *Nat. Neurosci.*, **18**, 75–86.

24. Igarashi M, Nozumi X, Wu LG, Zanacchi FC, Katona X, Barna XL, Xu P, Zhang M, Xue F, Boyden E. (2018) New observations in neuroscience using superresolution microscopy. *J. Neurosci.*, **38**, 9459–9467.
25. Choquet D, Sainlos M, Sibarita JB. (2021) Advanced imaging and labelling methods to decipher brain cell organization and function. *Nat. Rev. Neurosci.*, **22**, 237–255.
26. Avena-Koenigsberger A, Misic B, Sporns O. (2018) Communication dynamics in complex brain networks. *Nat. Rev. Neurosci.*, **19**, 17–33.
27. Cizeron M, Qiu Z, Koniaris B, Gokhale R, Komiyama NH, Fransén E, Grant SGN. (2020) A brainwide atlas of synapses across the mouse life span. *Science*, **369**, 270–275.
28. Martel JC, Gatti McArthur S. (2020) Dopamine Receptor Subtypes, Physiology and Pharmacology: New Ligands and Concepts in Schizophrenia. *Front. Pharmacol.*, **11**, 1–17.
29. Liu C, Goel P, Kaeser PS. (2021) Spatial and temporal scales of dopamine transmission. *Nat. Rev. Neurosci.*, **22**, 345–358.
30. Beaulieu J-M, Espinoza S, Gainetdinov RR. (2015) Dopamine receptors - IUPHAR Review 13. *Br. J. Pharmacol.*, **172**, 1–23.
31. Jones-Tabah J, Mohammad H, Paulus EG, Clarke PBS, Hébert TE. (2022) The Signaling and Pharmacology of the Dopamine D1 Receptor. *Front. Cell. Neurosci.*, **15**, 568.
32. Ramachandraiah CT, Subramaniam N, Tancer M. (2009) The story of antipsychotics: Past and present. *Indian J. Psychiatry*, **51**, 324–326.
33. Lally J, MacCabe JH. (2015) Antipsychotic medication in schizophrenia: a review. *Br. Med. Bull.*, **114**, 169–179.
34. Roth BL, Sheffler DJ, Kroeze WK. (2004) Magic shotguns versus magic bullets: selectively non-selective drugs for mood disorders and schizophrenia. *Nat. Rev. Drug Discov.*, **3**, 353–359.
35. Bancroft, B.S. G. (1998) Binding of [3H]PD 128907, a Putatively Selective Ligand for the D3 Dopamine Receptor, in Rat Brain: A Receptor Binding and Quantitative

Autoradiographic Study. *Neuropsychopharmacology*, **18**, 305–316.

36. Pottel J, Armstrong D, Zou L, Fekete A, Huang X-P, Torosyan H, Bednarczyk D, Whitebread S, Bhhatarai B, Liang G, Jin H, Ghaemi SN, Slocum S, Lukacs K V., Irwin JJ, Berg EL, Giacomini KM, Roth BL, Shoichet BK, Urban L. (2020) The activities of drug inactive ingredients on biological targets. *Science*, **369**, 403–413.
37. Madras BK. (2013) History of the discovery of the antipsychotic dopamine D2 receptor: A basis for the dopamine hypothesis of schizophrenia. *J. Hist. Neurosci.*, **22**, 62–78.
38. Tandon R. (2011) Antipsychotics in the Treatment of Schizophrenia. *J. Clin. Psychiatry*, **72 Suppl**, 4–8.
39. Sykes DA, Moore H, Stott L, Holliday N, Javitch JA, Lane JR, Charlton SJ. (2017) Extrapyramidal side effects of antipsychotics are linked to their association kinetics at dopamine D2 receptors. *Nat. Commun.*, **8**, 763.
40. Klein Herenbrink C, Sykes DA, Donthamsetti P, Canals M, Coudrat T, Shonberg J, Scammells PJ, Capuano B, Sexton PM, Charlton SJ, Javitch JA, Christopoulos A, Lane JR. (2016) The role of kinetic context in apparent biased agonism at GPCRs. *Nat. Commun.*, **7**, 10842.
41. Urs NM, Gee SM, Pack TF, McCorvy JD, Evron T, Snyder JC, Yang X, Rodriguiz RM, Borrelli E, Wetsel WC, Jin J, Roth BL, O'Donnell P, Caron MG. (2016) Distinct cortical and striatal actions of a β-arrestin–biased dopamine D2 receptor ligand reveal unique antipsychotic-like properties. *Proc. Natl. Acad. Sci.*, **113**, E8178–E8186.
42. Kiss B, Horváth A, Némethy Z, Schmidt É, Laszlovszky I, Bugovics G, Fazekas K, Hornok K, Orosz S, Gyertyán I, Ágai-Csongor É, Domány G, Tihanyi K, Adham N, Szombathelyi Z. (2010) Cariprazine (RGH-188), a Dopamine D 3 Receptor-Preferring, D 3 /D 2 Dopamine Receptor Antagonist–Partial Agonist Antipsychotic Candidate: In Vitro and Neurochemical Profile. *J. Pharmacol. Exp. Ther.*, **333**, 328–340.
43. Kiss B, Laszlovszky I, Krámos B, Visegrády A, Bobok A, Lévay G, Lendvai B, Román V. (2021) Neuronal dopamine D3 receptors: Translational implications for preclinical research and CNS disorders. *Biomolecules*, **11**, 1–39.
44. Earley W, Guo H, Daniel D, Nasrallah H, Durgam S, Zhong Y, Patel M, Barabássy

Á, Szatmári B, Németh G. (2019) Efficacy of cariprazine on negative symptoms in patients with acute schizophrenia: A post hoc analysis of pooled data. *Schizophr. Res.*, **204**, 282–288.

45. Earley W, Burgess MV, Rekeda L, Dickinson R, Szatmári B, Németh G, McIntyre RS, Sachs GS, Yatham LN. (2019) Cariprazine treatment of bipolar depression: A randomized double-blind placebo-controlled phase 3 study. *Am. J. Psychiatry*, **176**, 439–448.
46. Durgam S, Earley W, Li R, Li D, Lu K, Laszlovszky I, Fleischhacker WW, Nasrallah HA. (2016) Long-term cariprazine treatment for the prevention of relapse in patients with schizophrenia: A randomized, double-blind, placebo-controlled trial. *Schizophr. Res.*, **176**, 264–271.
47. Zimnisky R, Chang G, Gyertyán I, Kiss B, Adham N, Schmauss C. (2013) Cariprazine, a dopamine D3-receptor-preferring partial agonist, blocks phencyclidine-induced impairments of working memory, attention set-shifting, and recognition memory in the mouse. *Psychopharmacology (Berl).*, **226**, 91–100.
48. Duric V, Banasr M, Franklin T, Lepack A, Adham N, Kiss B, Gyertyán I, Duman RS. (2017) Cariprazine Exhibits Anxiolytic and Dopamine D3 Receptor-Dependent Antidepressant Effects in the Chronic Stress Model. *Int. J. Neuropsychopharmacol.*, **20**, 788–796.
49. Allikalt A, Rinken A. (2015) Characterization of ligand binding to dopamine receptors with fluorescence anisotropy based assay. *Springerplus*, **4**, 1–32.
50. Allikalt A, Laasfeld T, Ilisson M, Kopanchuk S, Rinken A. (2021) Quantitative analysis of fluorescent ligand binding to dopamine D3 receptors using live-cell microscopy. *FEBS J.*, **288**, 1514–1532.
51. Nebel N, Maschauer S, Kuwert T, Hocke C, Prante O. (2016) In Vitro and In Vivo Characterization of Selected Fluorine-18 Labeled Radioligands for PET Imaging of the Dopamine D3 Receptor. *Molecules*, **21**, 1144.
52. Allikalt A, Kopanchuk S, Rinken A. (2018) Implementation of fluorescence anisotropy-based assay for the characterization of ligand binding to dopamine D1 receptors. *Eur. J. Pharmacol.*, **839**, 40–46.
53. Tóth AD, Garger D, Prokop S, Soltész-Katona E, Várnai P, Balla A, Turu G, Hunyady L. (2021) A general method for quantifying ligand binding to unmodified

receptors using Gaussia luciferase. *J. Biol. Chem.*, **296**, 100366.

54. Wacker D, Stevens RC, Roth BL. (2017) How Ligands Illuminate GPCR Molecular Pharmacology. *Cell*, **170**, 414–427.
55. Boström J, Brown DG, Young RJ, Keserü GM. (2018) Expanding the medicinal chemistry synthetic toolbox. *Nat. Rev. Drug Discov.*, **17**, 709–727.
56. Renaud JP, Chari A, Ciferri C, Liu WT, Rémigy HW, Stark H, Wiesmann C. (2018) Cryo-EM in drug discovery: Achievements, limitations and prospects. *Nat. Rev. Drug Discov.*, **17**, 471–492.
57. García-Nafría J, Tate CG. (2021) Structure determination of GPCRs: cryo-EM compared with X-ray crystallography. *Biochem. Soc. Trans.*, **49**, 2345–2355.
58. García-Nafría J, Nehmé R, Edwards PC, Tate CG. (2018) Cryo-EM structure of the serotonin 5-HT1B receptor coupled to heterotrimeric Go. *Nature*, **558**, 620–623.
59. Prokop S, Ábrányi-Balogh P, Barti B, Vámosi M, Zöldi M, Barna L, Urbán GM, Tóth AD, Dudok B, Egyed A, Deng H, Leggio GM, Hunyady L, van der Stelt M, Keserű GM, Katona I. (2021) PharmacoSTORM nanoscale pharmacology reveals cariprazine binding on Islands of Calleja granule cells. *Nat. Commun.*, **12**, 6505.
60. Fallon JH, Riley JN, Sipe JC, Moore RY. (1978) The islands of Calleja: Organization and connections. *J. Comp. Neurol.*, **181**, 375–395.
61. Ribak CE, Fallon JH. (1982) The island of Calleja complex of rat basal forebrain. I. Light and electron microscopic observations. *J. Comp. Neurol.*, **205**, 207–218.
62. Millhouse OE. (1987) Granule cells of the olfactory tubercle and the question of the islands of calleja. *J. Comp. Neurol.*, **265**, 1–24.
63. De Vente J, Hani L, Steinbusch HE, Steinbusch HWM. (2001) The three dimensional structure of the islands of Calleja: A single heterogenous cell complex. *Neuroreport*, **12**, 565–568.
64. Adjei S, Wesson DW. (2015) Laminar and spatial localization of the islands of Calleja in mice. *Neuroscience*, **287**, 137–143.
65. Wesson DW. (2020) The Tubular Striatum. *J. Neurosci.*, **40**, 7379–7386.
66. Stefan Dhein, Friedrich Wilhelm Mohr MD. (2006) 6.3.1 Radioligand Binding Studies in Cardiovascular Research (Saturation and Competition Binding Studies). in *Practical Methods in Cardiovascular Research*, pp. 723–783

67. Alexander SP, Christopoulos A, Davenport AP, Kelly E, Mathie A, Peters JA, Veale EL, Armstrong JF, Faccenda E, Harding SD, Pawson AJ, Southan C, Davies JA, Abbracchio MP, Alexander W, Al-Hosaini K, Bäck M, Barnes NM, Bathgate R, Beaulieu J, Bernstein KE, Bettler B, Birdsall NJM, Blaho V, Boulay F, Bousquet C, Bräuner-Osborne H, Burnstock G, Caló G, Castaño JP, Catt KJ, Ceruti S, Chazot P, Chiang N, Chini B, Chun J, Cianciulli A, Civelli O, Clapp LH, Couture R, Csaba Z, Dahlgren C, Dent G, Singh KD, Douglas SD, Dournaud P, Eguchi S, Escher E, Filardo EJ, Fong T, Fumagalli M, Gainetdinov RR, Gasparo M de, Gerard C, Gershengorn M, Gobeil F, Goodfriend TL, Goudet C, Gregory KJ, Gundlach AL, Hamann J, Hanson J, Hauger RL, Hay DL, Heinemann A, Hollenberg MD, Holliday ND, Horiuchi M, Hoyer D, Hunyady L, Husain A, IJzerman AP, Inagami T, Jacobson KA, Jensen RT, Jockers R, Jonnalagadda D, Karnik S, Kaupmann K, Kemp J, Kennedy C, Kihara Y, Kitazawa T, Kozielewicz P, Kreienkamp H, Kukkonen JP, Langenhan T, Leach K, Lecca D, Lee JD, Leeman SE, Leprince J, Li XX, Williams TL, Lolait SJ, Lupp A, Macrae R, Maguire J, Mazella J, McArdle CA, Melmed S, Michel MC, Miller LJ, Mitolo V, Mouillac B, Müller CE, Murphy P, Nahon J, Ngo T, Norel X, Nyimanu D, O'Carroll A-M, Offermanns S, Panaro MA, Parmentier M, Pertwee RG, Pin J, Prossnitz ER, Quinn M, Ramachandran R, Ray M, Reinscheid RK, Rondard P, Rovati GE, Ruzza C, Sanger GJ, Schöneberg T, Schulte G, Schulz S, Segaloff DL, Serhan CN, Stoddart LA, Sugimoto Y, Summers R, Tan VP, Thal D, Thomas W, Timmermans PBMWM, Tirupula K, Tulipano G, Unal H, Unger T, Valant C, Vanderheyden P, Vaudry D, Vaudry H, Vilardaga J, Walker CS, Wang JM, Ward DT, Wester H, Willars GB, Woodruff TM, Yao C, Ye RD. (2021) THE CONCISE GUIDE TO PHARMACOLOGY 2021/22: G protein-coupled receptors. *Br. J. Pharmacol.*, **178 Suppl**, S27–S156.

68. Hoffmann C, Castro M, Rinken A, Leurs R, Hill SJ, Vischer HF. (2015) Ligand Residence Time at G-protein–Coupled Receptors—Why We Should Take Our Time To Study It. *Mol. Pharmacol.*, **88**, 552–560.

69. Vauquelin G, Van Liefde I, Swinney DC. (2015) Radioligand binding to intact cells as a tool for extended drug screening in a representative physiological context. *Drug Discov. Today Technol.*, **17**, 28–34.

70. Vanderheyden PML, Benachour N. (2017) Influence of the cellular environment on ligand binding kinetics at membrane-bound targets. *Bioorg. Med. Chem. Lett.*, **27**, 3621–3628.
71. Wan Q, Okashah N, Inoue A, Nehme R, Carpenter B, Tate CG, Lambert NA. (2018) Mini G protein probes for active G protein–coupled receptors (GPCRs) in live cells. *J. Biol. Chem.*, **293**, 7466.
72. Raquel Miquel M, Segura V, Ali Z, D'Ocon MP, McGrath JC, Daly CJ. (2005) 3-D image analysis of fluorescent drug binding. *Mol. Imaging*, **4**, 40–52.
73. Daly CJ, Ross RA, Whyte J, Henstridge CM, Irving AJ, McGrath JC. (2010) Fluorescent ligand binding reveals heterogeneous distribution of adrenoceptors and "cannabinoid-like" receptors in small arteries. *Br. J. Pharmacol.*, **159**, 787–796.
74. Jones SA, Shim SH, He J, Zhuang X. (2011) Fast, three-dimensional super-resolution imaging of live cells. *Nat. Methods*, **8**, 499–505.
75. Fricke F, Malkusch S, Wangorsch G, Greiner JF, Kaltschmidt B, Kaltschmidt C, Widera D, Dandekar T, Heilemann M. (2014) Quantitative single-molecule localization microscopy combined with rule-based modeling reveals ligand-induced TNF-R1 reorganization toward higher-order oligomers. *Histochem. Cell Biol.*, **142**, 91–101.
76. York AL, Zheng JQ. (2017) Super-Resolution Microscopy Reveals a Nanoscale Organization of Acetylcholine Receptors for Trans-Synaptic Alignment at Neuromuscular Synapses. *eNeuro*, **4**, ENEURO.0232-17.2017.
77. Szalai AM, Armando NG, Barabas FM, Stefani FD, Giordano L, Bari SE, Cavasotto CN, Silberstein S, Aramendía PF. (2018) A fluorescence nanoscopy marker for corticotropin-releasing hormone type 1 receptor: Computer design, synthesis, signaling effects, super-resolved fluorescence imaging, and: In situ affinity constant in cells. *Phys. Chem. Chem. Phys.*, **20**, 29212–29220.
78. Ast J, Arvaniti A, Fine NHF, Nasteska D, Ashford FB, Stamataki Z, Koszegi Z, Bacon A, Jones BJ, Lucey MA, Sasaki S, Brierley DI, Hastoy B, Tomas A, D'Agostino G, Reimann F, Lynn FC, Reissaus CA, Linnemann AK, D'Este E, Calebiro D, Trapp S, Johnsson K, Podewin T, Broichhagen J, Hodson DJ. (2020) Super-resolution microscopy compatible fluorescent probes reveal endogenous

glucagon-like peptide-1 receptor distribution and dynamics. *Nat. Commun.*, **11**, 467.

79. Sarott RC, Westphal M V., Pfaff P, Korn C, Sykes DA, Gazzi T, Brennecke B, Atz K, Weise M, Mostinski Y, Hompluem P, Koers E, Miljuš T, Roth NJ, Asmelash H, Vong MC, Piovesan J, Guba W, Rufer AC, Kusznir EA, Huber S, Raposo C, Zirwes EA, Osterwald A, Pavlovic A, Moes S, Beck J, Benito-Cuesta I, Grande T, Ruiz de Martín Esteban S, Yeliseev A, Drawnel F, Widmer G, Holzer D, van der Wel T, Mandhair H, Yuan C-Y, Drobyski WR, Saroz Y, Grimsey N, Honer M, Fingerle J, Gawrisch K, Romero J, Hillard CJ, Varga Z V., van der Stelt M, Pacher P, Gertsch J, McCormick PJ, Ullmer C, Oddi S, Maccarrone M, Veprintsev DB, Nazaré M, Grether U, Carreira EM. (2020) Development of High-Specificity Fluorescent Probes to Enable Cannabinoid Type 2 Receptor Studies in Living Cells. *J. Am. Chem. Soc.*, **142**, 16953–16964.
80. Mlodzianoski MJ, Cheng-Hathaway PJ, Bemiller SM, McCray TJ, Liu S, Miller DA, Lamb BT, Landreth GE, Huang F. (2018) Active PSF shaping and adaptive optics enable volumetric localization microscopy through brain sections. *Nat. Methods*, **15**, 583–586.
81. Bon P, Linarès-Loyez J, Feyeux M, Alessandri K, Lounis B, Nassoy P, Cognet L. (2018) Self-interference 3D super-resolution microscopy for deep tissue investigations. *Nat. Methods*, **15**, 449–454.
82. Nehme E, Freedman D, Gordon R, Ferdman B, Weiss LE, Alalouf O, Naor T, Orange R, Michaeli T, Shechtman Y. (2020) DeepSTORM3D: dense 3D localization microscopy and PSF design by deep learning. *Nat. Methods*, **17**, 734–740.
83. Xu F, Ma D, MacPherson KP, Liu S, Bu Y, Wang Y, Tang Y, Bi C, Kwok T, Chubykin AA, Yin P, Calve S, Landreth GE, Huang F. (2020) Three-dimensional nanoscopy of whole cells and tissues with in situ point spread function retrieval. *Nat. Methods*, **17**, 531–540.
84. Zhang T, Hatcher JM, Teng M, Gray NS, Kostic M. (2019) Recent Advances in Selective and Irreversible Covalent Ligand Development and Validation. *Cell Chem. Biol.*, **26**, 1486–1500.
85. Stoddart LA, Kindon ND, Otun O, Harwood CR, Patera F, Veprintsev DB,

Woolard J, Briddon SJ, Franks HA, Hill SJ, Kellam B. (2020) Ligand-directed covalent labelling of a GPCR with a fluorescent tag in live cells. *Commun. Biol.*, **3**, 722.

86. Weichert D, Kruse AC, Manglik A, Hiller C, Zhang C, Hubner H, Kobilka BK, Gmeiner P. (2014) Covalent agonists for studying G protein-coupled receptor activation. *Proc. Natl. Acad. Sci.*, **111**, 10744–10748.
87. Schwalbe T, Kaindl J, Hübner H, Gmeiner P. (2017) Potent haloperidol derivatives covalently binding to the dopamine D2 receptor. *Bioorg. Med. Chem.*, **25**, 5084–5094.
88. Donthamsetti PC, Winter N, Schönberger M, Levitz J, Stanley C, Javitch JA, Isacoff EY, Trauner D. (2017) Optical Control of Dopamine Receptors Using a Photoswitchable Tethered Inverse Agonist. *J. Am. Chem. Soc.*, **139**, 18522.
89. Lorincz A, Nusser Z. (2008) Specificity of Immunoreactions: The Importance of Testing Specificity in Each Method. *J. Neurosci.*, **28**, 9083–9086.
90. Bradbury A, Plückthun A. (2015) Reproducibility: Standardize antibodies used in research. *Nature*, **518**, 27–29.
91. Uhlen M, Bandrowski A, Carr S, Edwards A, Ellenberg J, Lundberg E, Rimm DL, Rodriguez H, Hiltke T, Snyder M, Yamamoto T. (2016) A proposal for validation of antibodies. *Nat. Methods*, **13**, 823–827.
92. Chien EYT, Liu W, Zhao Q, Katritch V, Han GW, Hanson MA, Shi L, Newman AH, Javitch JA, Cherezov V, Stevens RC. (2010) Structure of the human dopamine D3 receptor in complex with a D2/D3 selective antagonist. *Science*, **330**, 1091–5.
93. Xu P, Huang S, Mao C, Krumm BE, Zhou XE, Tan Y, Huang XP, Liu Y, Shen DD, Jiang Y, Yu X, Jiang H, Melcher K, Roth BL, Cheng X, Zhang Y, Xu HE. (2021) Structures of the human dopamine D3 receptor-Gi complexes. *Mol. Cell*, **81**, 1147-1159.e4.
94. Le Foll B, Wilson AA, Graff A, Boileau I, Di Ciano P. (2014) Recent methods for measuring dopamine D3 receptor occupancy in vivo: importance for drug development. *Front. Pharmacol.*, **5**, 161.
95. Doot RK, Dubroff JG, Labban KJ, Mach RH. (2019) Selectivity of probes for PET imaging of dopamine D3 receptors. *Neurosci. Lett.*, **691**, 18–25.
96. Yin J, Chen K-YM, Clark MJ, Hijazi M, Kumari P, Bai X, Sunahara RK, Barth P,

Rosenbaum DM. (2020) Structure of a D2 dopamine receptor–G-protein complex in a lipid membrane. *Nature*, **584**, 125–129.

97. Ishiwata K, Ogi N, Tanaka A, Senda M. (1999) Quantitative ex vivo and in vitro receptor autoradiography using 11C- labeled ligands and an imaging plate: A study with a dopamine D2-like receptor ligand [11C]nemonapride. *Nucl. Med. Biol.*, **26**, 291–296.
98. Gurevich EV., Himes JW, Joyce JN. (1999) Developmental regulation of expression of the D3 dopamine receptor in rat nucleus accumbens and islands of Calleja. *J. Pharmacol. Exp. Ther.*, **289**, 587–98.
99. Stanwood GD, Artymyshyn RP, Kung MP, Kung HF, Lucki I, McGonigle P. (2000) Quantitative autoradiographic mapping of rat brain dopamine D3 binding with [125I]7-OH-PIPAT: Evidence for the presence of D3 receptors on dopaminergic and nondopaminergic cell bodies and terminals. *J. Pharmacol. Exp. Ther.*, **295**, 1223–1231.
100. Lemercier EC, Schulz BS, Heidmann EK, Kovács R, Gerevich Z. (2015) Dopamine D3 Receptors Inhibit Hippocampal Gamma Oscillations by Disturbing CA3 Pyramidal Cell Firing Synchrony. *Front. Pharmacol.*, **6**, 297.
101. Clarkson RL, Liptak AT, Gee SM, Sohal VS, Bender KJ. (2017) D3 receptors regulate excitability in a unique class of prefrontal pyramidal cells. *J. Neurosci.*, **37**, 5846–5860.
102. Shin S, Pribiag H, Lilascharoen V, Knowland D, Wang XY, Lim BK. (2018) Drd3 Signaling in the Lateral Septum Mediates Early Life Stress-Induced Social Dysfunction. *Neuron*, **97**, 195-208.e6.
103. Pribiag H, Shin S, Wang EH-J, Sun F, Datta P, Okamoto A, Guss H, Jain A, Wang XY, Freitas B De, Honma P, Pate S, Lilascharoen V, Li Y, Lim BK. (2021) Ventral pallidum DRD3 potentiates a pallido-habenular circuit driving accumbal dopamine release and cocaine seeking. *Neuron*, **109**, 2165-2182.e10.
104. Leggio GM, Torrisi SA, Mastrogiacomo R, Mauro D, Chisari M, Devroye C, Scheggia D, Nigro M, Geraci F, Pintori N, Giurdanella G, Costa L, Bucolo C, Ferretti V, Sortino MA, Ciranna L, De Luca MA, Mereu M, Managò F, Salomone S, Drago F, Papaleo F. (2021) The epistatic interaction between the dopamine D3 receptor and dysbindin-1 modulates higher-order cognitive functions in mice and

humans. *Mol. Psychiatry*, **26**, 1272–1285.

105. Mansouri E, Nobrega JN, Hill MN, Tyndale RF, Lee FS, Hendershot CS, Best LM, Di Ciano P, Balsevich G, Sloan ME, Kish SJ, Tong J, Le Foll B, Boileau I. (2020) D3 dopamine receptors and a missense mutation of fatty acid amide hydrolase linked in mouse and men: implication for addiction. *Neuropsychopharmacology*, **45**, 745–752.
106. Gurevich EV, Bordelon Y, Shapiro RM, Arnold SE, Gur RE, Joyce JN. (1997) Mesolimbic dopamine D3 receptors and use of antipsychotics in patients with schizophrenia: A postmortem study. *Arch. Gen. Psychiatry*, **54**, 225–232.

8. Bibliography of the candidate's publications

Publications related to the thesis:

1. Tóth AD, Garger D, **Prokop S**, Soltész-Katona E, Várnai P, Balla A, Turu G, Hunyady L. (2021) A general method for quantifying ligand binding to unmodified receptors using *Gaussia* luciferase. *J Biol Chem*, 296:100366. I.F.: 5.157
2. **Prokop S***, Ábrányi-Balogh P*, Barti B, Vámosi M, Zöldi M, Barna L, Urbán GM, Tóth AD, Dudok B, Egyed A, Deng H, Leggio GM, Hunyady L, van der Stelt M, Keserű GM*, Katona I. (2021) PharmacoSTORM nanoscale pharmacology reveals cariprazine binding on Islands of Calleja granule cells. *Nat Commun*, 212(1):6505.
   I.F.: 14.919

Publications unrelated to the thesis:

1. Szalai B, Hoffmann P, **Prokop S**, Erdélyi L, Várnai P, Hunyady L. (2014) Improved methodical approach for quantitative BRET analysis of G Protein Coupled Receptor dimerization. *PLoS One,* 9(10):e109503 I.F.: 3.234
2. Elek Z, Dénes R, **Prokop S**, Somogyi A, Yowanto H, Luo J, Souquet M, Guttman A, Rónai Z. (2016) Multicapillary gel electrophoresis based analysis of genetic variants in the WFS1 gene. *Electrophoresis*, 37(17-18):2313-21 I.F.: 2.744
3. **Prokop S**, Perry NA, Vishnivetskiy SA, Toth AD, Inoue A, Milligan G, Iverson TM, Hunyady L, Gurevich VV. (2017) Differential manipulation of arrestin-3 binding to basal and agonist-activated G protein-coupled receptors. *Cell Signal*, 36:98-107.
   I.F.: 3.487
4. Tóth AD*, **Prokop S***, Gyombolai P, Várnai P, Balla A, Gurevich VV, Hunyady L, Turu G. (2018) Heterologous phosphorylation-induced formation of a stability lock permits regulation of inactive receptors by β-arrestins. *J Biol Chem*, 293(3):876-892.
   I.F.: 4.106

DOI:10.14753/SE.2022.2679

9. Acknowledgements

I would like to thank all the former and current members of the laboratory of László Hunyady and István Katona who helped the present work with valuable discussions and technical help. I am thankful for the collaborative work of all members of the laboratory of György M. Keserű.

I would like to thank Bence Szalai for introducing me the field of GPCRs, and for his patient supervision. Furthermore, I am thankful for Nóra Németh, Mehmet Takar and Nicole Perry for teaching me laboratory skills, and for Zsolt Rónai, Todd R. Graham and Vsevolod V. Gurevich for mentoring my research work as an undergraduate student. I thank the continuous support and constructive criticism of András Tóth during my PhD. I would like to acknowledge with gratitude the support of István Katona and I thank him for being a consistent source of advice in science.

I am indebted for the microscopy support of the Microscopy Center at the Institute of Experimental Medicine and László Barna. My research studies were supported by the New National Excellence Program of the Ministry for Innovation and Technology (ÚNKP-20-3-II-SE-33, ÚNKP-19-3-III-SE-16 and ÚNKP_18-3-I-SE-13).

Finally, I thank the unconditional support of my family, without them, this project could have never been accomplished.